UNIVERSIDADE DE SÃO PAULO
INSTITUTO DE FÍSICA DE SÃO CARLOS

CAMILO ARTURO SUÁREZ BALLESTEROS

Smart nanomaterials based on photoactivated release of silver nanoparticles for bacterial control

São Carlos

2017

CAMILO ARTURO SUÁREZ BALLESTEROS

Smart nanomaterials based on the photoactivated release of silver nanoparticles for bacterial control

Thesis presented to the Graduate Program in Physics at the Instituto de Física de São Carlos, Universidade de São Paulo to obtain the degree of Doctor of Science.

Concentration area: Applied Physics
Option: Biomolecular Physics

Advisor: Prof. Dr. Valtencir Zucolotto
Coadvisor: Prof. Dr. Daniel Souza Corrêa

Corrected Version

São Carlos

2017

Cataloguing data reviewed by the Library and Information Service
of the IFSC, with information provided by the author

Ballesteros, Camilo Arturo Suarez
Smart nanomaterials based on the photoactivated release of silver nanoparticles for bacterial control / Camilo Arturo Suarez Ballesteros; advisor Valtencir Zucolotto; co-advisor Daniel Souza Corrêa - reviewed version -- São Carlos 2017.
101 p.

Thesis (Doctorate - Graduate Program in Biomolecular Physics) -- Instituto de Física de São Carlos, Universidade de São Paulo - Brasil , 2017.

1. Plasmonic nanoparticles. 2. Nanocapsules. 3. Photoactivation. 4. Antibacterial properties. 5. Langmuir monolayers. I. Zucolotto, Valtencir, advisor. II. Souza Corrêa, Daniel, co-advisor. III. Title.

To my parents, Luz Aida and Carlos, and my brothers Diego and Carlos Ivan, for being present in every moment of my life.

Acknowledgements

I want to thank to God for all opportunities to learn of all occasions and give me all the necessary. I would like to thank to all people and institutions that have contributed direct or indirect during my life.

I deeply acknowledge my parents Luz Aida and Carlos and my brothers Diego and Carlos Ivan for all support, encouraging me in all my decisions and their unconditional love.

I acknowledge my advisor prof. Dr. Valtencir Zucolotto for the opportunity, contributions and freedom during the development of my PhD project.

I thank my coadvisor prof. Dr. Daniel Souza Correa, for the contributions and teaching during my PhD project.

I thank to Capes to the financial support during PhD.

I thank everybody in the GNano lab working: Jaque, Romeu and Nilzeli.

I thank the technicians and staff of Embrapa Instrumentation.

I thank my colleagues from GNano: Juliana, Lais Brazaca, Jaque, Valeria, Idelma, Nirton, Lorena, Paula, Henrique, Fran, Cris, Lais Ribovisk, Helena, Adrislaine, Isa, Olavo, Abilene.

I am grateful to my close friends Diego, Edward and Jackson for their help and support.

Finally, I would like to thank Universidade de Sao Paulo, especially Instituto de Fisica de Sao Carlos (IFSC) and Embrapa instrumentation for the exceptional infrastructure and education that I received in my master and PhD.

“You can’t depend on your eyes when your imagination is out of focus”

Charles Darwin

ABSTRACT

BALLESTEROS, C. S. **Smart nanomaterials based on the photoactivated release of silver nanoparticles for bacterial control**. 2017. 101p. Thesis (Doctor in Science) – Instituto de Física de São Carlos, Universidade de São Paulo, São Carlos, 2017.

Smart nanomaterials can selectively respond to a stimulus and consequently be activated in specific conditions, as a result of their interaction with electromagnetic radiation, biomolecules, pH change, etc. These nanomaterials can be produced through distinct routes and be used in artificial skin, drug delivery, and other biomedical applications. In this thesis, two smart nanosystems were developed, viz., i) nanocapsules formed by aniline (A) and chitosan (CS) (A-CS) containing silver nanoparticles (AgNPs), with an average size of 78 ± 19 nm, and ii) polycaprolactone (PCL) nanofibers, fabricated by the electrospinning technique containing AgNP into their bulk, with a diameter of 417 ± 14 nm. A novel system, based on the incorporation of the as-prepared nanocapsules onto the surface of PCL nanofibers containing AgNps (antibacterial mats), was also developed. The methodology employed avoids the direct contact of silver nanoparticles with the host and optimizes its release to the surrounding environment. The AgNPs release was triggered by exposing the nanocapsules to light at 405 nm. Consequently, the electronic energy vibration resulting from the interaction of the irradiation with the surface plasmon band (SPR) of AgNps, breaking the hydrogen bonds of the nanocapsules and releasing of AgNPs at a time of 150 s. To understand the perturbation of AgNps-Nanocapsules against bacteria, membrane models using Langmuir technique with the phospholipids 1,2-dipalmitoyl-sn-glycero-3-phospho-(1'-rac-glycerol) (DPPG) and 1,2-dimyristoyl-sn-glycero-3-phosphoethanolamine (DMPE) were employed, which are the main components of cell membrane of *Escherichia coli (E. coli)*. The results suggest that DPPG has more influence on the incorporation of the nanoparticles on the cell membrane. The antibacterial properties of the nanofibers/nanomaterials mats towards *E. coli* and *Staphylococcus aureus* (*S. aureus*) were investigated using the Agar diffusion test for 8 samples. The experiments revealed that the samples based on nanofibers/nanocapsules and irradiation presented a radius of inhibition of 2.58 ± 0.28 mm for *S. aureus* and 1.78 ± 0.49 mm for *E. coli*. This nanosystem showed to be highly interesting for biomedical applications.

Keywords: Plasmonic nanoparticles. Nanocapsules. Photoactivation. Antibacterial properties.

RESUMO

BALLESTEROS, C. S. **Nanomateriais inteligentes baseados na liberação fotoativada de nanopartículas de prata para controle bacteriano**. 2017. 101p. Tese (Doutorado em Ciências) – Instituto de Física de São Carlos, Universidade de São Paulo, São Carlos, 2017.

Nanomateriais inteligentes podem responder seletivamente a um estímulo e consequentemente ser ativados em condições específicas, como resultado da sua interação com a radiação eletromagnética, mudança do pH, campo magnético, etc. Esses materiais podem ser produzidos através de distintas rotas e utilizados em aplicações como pele artificial, liberação de fármacos, e outras aplicações biomédicas. Nessa tese, dois nanossistemas inteligentes foram desenvolvidos, a saber: i) nanocápsulas formadas por anilina (A) e quitosana (CS) (A-CS) contendo nanopartículas de prata (AgNps), com um tamanho médio de 78 ± 19 nm, e ii) nanofibras de policaprolactona (PCL), fabricadas pela técnica de eletrofiação contendo AgNps em seu interior, com diâmetro de 417 ± 14 nm. Um terceiro sistema foi desenvolvido, baseado na incorporação das nanocápsulas na superfície das nanofibras de PCL contendo AgNps (manta antibacteriana). A metodologia utilizada evita o contato direto das nanopartículas de prata com o hospedeiro e otimiza sua liberação no meio ambiente. As AgNps liberadas foram acionadas pela exposição das nanocápsulas à um fonte de luz em 405 nm. Consequentemente, a vibração da energia eletrônica resultante da interação da irradiação com a banda plasmônica de superfície (SPR) das AgNps, quebra as ligações de hidrogênio da nanocápsula e libera as AgNps no meio em um tempo de 150 s. Para entender a perturbação das AgNps-nanocapsulas contra as bactérias, modelos de membrana foram usados através da técnica de Langmuir com os fosfolipídios 1,2-dipalmitoil-sn-glicero-3-fosfo-(1'-rac-glicerol) (DPPG) and 1,2-dimiristoil-sn-glicero-3-fosfoetanolamina (DMPE), que são os principais componentes da membrana celular de *Escherichia coli (E. coli)*. Os resultados sugerem que DPPG tem mais influência na incorporação das nanopartículas na membrana celular. As propriedades antibacterianas das mantas de nanofibras/nanomateriais contra *E. coli* e *Staphylococus aureus (S. aureus)* foram investigadas usando o teste de difusão Agar em 8 grupos, o qual revelou que o grupo contendo a nanofibra/nanocapsula e irradiação apresentou um raio de inibição de 2.58 ± 0.28 mm para *S. aureus* e 1.78 ± 0.49 mm

para *E. coli*. Este nanossistema mostrou ser altamente interessante para aplicações biomédicas.

Palavras-chave: Nanopartículas plasmônicas. Nanocápsulas. Fotoactivação. Antibacterial.

LIST OF FIGURES

LIST OF ABREVIATIONS AND ACRONYMS

A	aniline
AgNps	silver nanoparticles
AgNps Nanocapsules	nanocapsules loaded with silver nanoparticles
AgNps-CS	Ag nanoparticles-chitosan
A-CS	aniline-chitosan
AP	ascorbyl palmitate
cm	centimeter
cP	centipoises
CLSI	Clinical & Laboratory Standards Institute
CS	chitosan
DPPG	1,2-dipalmitoyl-sn-glycero-3-phospho-(1'-rac-glycerol
DMPE	1,2-dimyristoyl-sn-glycero-3-phosphoethanolamine
DLS	dynamic light scattering
DMF	aimethylformamide
DCM	dichloromethane
EDX	Energy-dispersive X-ray spectroscopy
E. coli	*Escherichia coli*
FT IR	Fourier transform infrared spectroscopy
FESEM	field-emission Scanning Electron Microscopy
Laser	light amplification by stimulated emission of radiation
Led	light-emitting diode
LSPR	localized surface Plasmon resonance
MIC	minimum inhibition concentration
NC	AgNps Nanocapsules
PCL Nfs	Polycaprolactone nanofibers

PDI	polydispersity index
PCL	polycaprolactone
PEG	polyethylene glycol
PLGA	poly(lactic-co-glycolic acid)
S. aurius	Staphylococcus aureus
s	seconds
SPB	surface plasmon band
SPR	surface plasmon resonance
UV-Vis	ultraviolet-visible
VLT	visible light therapy

LIST OF SYMBOLS

ε	dielectric function
ε_r	real part
ε_i	imaginary part
λ	wavelength
C_{ext}	extinction cross section
r	radius
ε_m	relative dielectric constant
Ag+	silver ions
Π	surface pressure
γ_0	subphase with pure water
γ	subphase with the film

CONTENTS

1 Introduction

Considerable attention has been devoted to the development of smart nanomaterials that can release in a slow and/or controlled manner substances aiming at antimicrobial applications.[1-2] These nanomaterials can be activated in specific conditions as upon interaction with electromagnetic radiation, pH, biomolecules, metallic and polymeric materials.[3 - 5] For many years, antimicrobial drugs have been used to inhibit or kill microbes. However, microbial resistance to these drugs has been found, reducing their effectiveness and becoming a public health problem.[6]

One of the most promising strategies for fighting against antimicrobial resistance is the use of smart nanomaterials,[7-8] for instance, polymeric nanocapsules, which can encapsulate several substances and release them on demand at a later stage.[9 - 12] For that purpose, challenges need to be overcome to produce reliable and uniform nanocapsules with properties that can be altered by applying a remote stimulus, such as irradiation.[5, 13-14] Polymeric nanocapsules loaded with metallic nanoparticles can be irradiated at a specific wavelength, generating local electronic vibration, which leads to changes in the polymeric structure, releasing the nanoparticles to the surrounding environment.[15 - 17] Among nanoparticles with antibacterial properties, silver nanoparticles stand out, once silver ions released from the crystalline core can produce a chemical disequilibrium in the bacterial cell.[18] In addition, the nanocapsules degradation yields to non-toxic products for the environment, which is a fundamental prerequisite to biomedical applications.[19 - 21]

Nanofibers are also an interesting type of nanomaterial for antibacterial application,[22] once they have morphological characteristics similar to extracellular proteins and biofilm structures that can be configured in different ways, and also allow their surface and bulk modification with smart nanostructures and biomolecules.[23 - 24] Consequently, it is possible to fabricate antibacterial nanofiber mats activated by external agents as pH, energy, degradation and diffusional processes.[25] These nanofiber mats configurations have shown to be an interesting alternative to the prevention of infections and sterilization of medical

instruments.[26 - 27] The mechanisms of actions are mainly ruled by interaction of the active substance with the cell membrane and subsequent internalization to cause the cell death.

To understand the mechanism of action of smart nanomaterials inside cells, it is important to determine their behavior with the cell membrane. For such investigation, the Langmuir technique[28] is a viable strategy, once it allows to build phospholipids monolayers of lipids presented in cell membrane, mimicking a membrane model to study the interaction between nanomaterial and membrane.[29] This technique makes possible to infer the nanomaterials organization in the subphase and changes induced in the surface structure.[30] Moreover, it allows to obtain information on the interaction of molecules with the nanomaterial at the interface.[31] Consequently, this process allows determining any possible toxic effects arising from the interaction.[32]

In this thesis we present a smart nanomaterial based on nanocapsules formed by cross-linking between functional groups of aniline (A) and chitosan (CS) (A-CS), containing silver nanoparticles, which were incorporated onto the surface of electrospun nanofibers. The developed material has antibacterial properties, since silver ions can be released in the surrounding environment through light irradiation for antibacterial purposes. Hence, this thesis explores three main subjects:

In **Chapter 2,** it is discussed the methodology through which AgNps-nanocapsules were synthesized and incorporated into polycaprolactone nanofibers (PCL Nfs). The AgNps-Nanocapsule was synthetized by the cross-linking between aniline(A) and chitosan(CS) in hybrid polymeric nanocapsules. The AgNps-Nanocapsule is shown to have optimal stability at pH 3.0 to 7.4, with a surface plasmon band centered at 405 nm. The PCL Nfs are fabricated by electrospining technique, and showed good homogeneity and optimal behavior in biological systems.

In **Chapter 3**, it is investigated the release of AgNps when the AgNps-nanocapsules are irradiated with a 405nm diode laser. Furthermore, the PCL Nfs are functionalized with AgNps-nanocapsules (antibacterial mats) and activated by irradiation with 405 nm light. The antibacterial capacity was investigated by agar diffusion test for *Gram-positive Staphylococcus aureus* and *Gram-negative Escherichia coli.*

In **Chapter 4**, we report the kinetics of AgNps release when the nanocapsules are irradiated by a 405 nm diodo LED. The minimum inhibitory concentration (MIC) of the

AgNps-nanocapsule dispersion was determined for Gram-negative *E coli*. In addition, the behavior of these nanomaterials was studied using membrane models by the Langmuir technique, using phospholipids DPPG and DMPE, which are the main components of cell membrane of Escherichia coli.

2 Synthesis and characterization of AgNps-Nanocapsules and Electrospun Nanofibers

2.1 Smart Nanosystems

Nanomedicine, a subject of nanotechnology, concerns to the investigation of the interactions between the biological systems and materials at the nanometer scale. Biological properties may change at nanoscale, covering systemic biodistribution, cellular trafficking, and mechanisms of biodegradation.[33] Materials properties, including physico-chemical, magnetic, electronic and optical properties[34] - [35] can also change at the nanoscale. Over the last years, two generations of nanomaterials have been used in host organism such as cells. The first generation of nanomaterials uses the physical-chemical characteristics such as size, shape and surface chemistry, but without activation of signaling-mechanisms on the host, to improve diagnosis or therapeutic capabilities.[36] This diagnostic requires simplicity, quick response, tolerability and selectivity to be used in patients.[33, 37] The second generation of smart nanosystems are inspired by nature, biomimetizing their physico-chemical properties such as the camouflage of the membrane cells, adhesion of the mussels, virus targeting, etc.[38] The biomimetization is used as a mechanism to avoid or allow the interaction with the host organisms.[39] These nanosystems can explore the host environment and react autonomously with external or internal stimulus to yield a diagnosis, regeneration tissue and/or treatment of diseases.[40] The stimulus change the nanoparticles behavior, for example, leading to degradation, swelling, activation of biomolecules, or recruitment of biological cascade.[41]

Nanomaterials are described within two classes of smart nanosystems that communicate with living hosts.[39] The first nanosystems are sensors that respond to the biological environment and disease conditions such as redox potential, pH, enzymatic activity, homeostatic pathways.[34] The second class of smart nanosystems has the ability of communicating with the host environment.[42] This behavior upon the environment is accomplished by administering stimulus, e.g. electromagnetic, heat, electrocatalytic, ultrasound, nanosystem themselves, and drugs.[39] When a stimulus is applied, it can change the behavior of the nanosystem-target (nanosystem-nanosystem or nanosystem-host) creating an interchange, recruitment, or amplification according to the application.[39, 43]

2.2 Nanocapsular structures

Among smart nanomaterials with interesting biomedical and industrial application are the nanocapsular structures.[44] Nanocapsular structures can be defined as nano-vesicular systems that exhibit a core-shell structure in which the *active substance* is confined to a reservoir or within a cavity surrounded by a polymer membrane or coating.[43] Nanocapsular structures can be separated in three groups, namely nanocapsules, nanospheres and nanogels.[45 - 46]

Nanocapsules are vesicular systems in which the active substance is confined to an aqueous or oil cavity surrounded by a single polymeric membrane,[47] as displayed in Figure 2.1a. Nanospheres are polymer systems in which the active substance is dispersed throughout the nanoparticles,[48] Figure 2.1b. Other type of nanocapsule is the nanogels. They are defined as aqueous dispersion of hydrogels particles formed by physically or chemically cross-linked polymer networks of nanoscale size,[45, 49] Figure 2.1c.

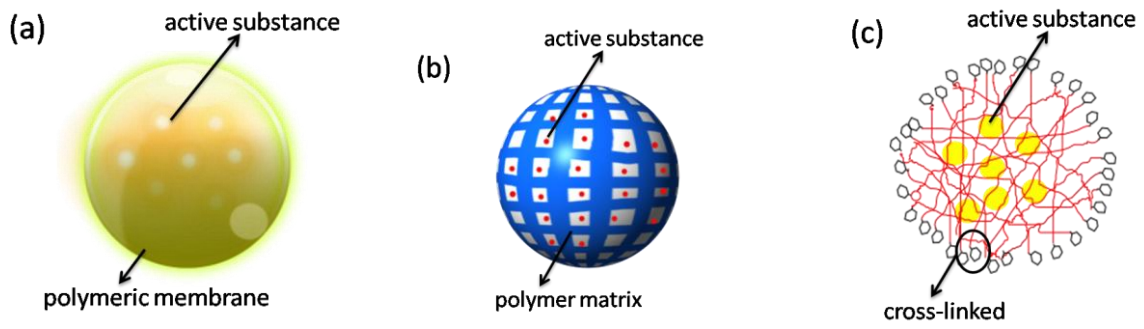

Figure 2.1 - Schematic representation of (a) Nanocapsule, (b) Nanosphere and (c) Nanogel.

Source: By the author

The release mechanism of these nanosystems can be studied by three distinct methods in which the chemical conformations is altered by switching reaction, disintegration of chemical cross-links and triggered depolymerization of the shell, as follows:[43, 50]

Switching: The configuration of the shell is altered by external stimulus as electricity, light and chemical, producing changes in chemical bonds, which initiates the release of active substances.[50]

Cross-link removal: It is the disintegration of the shell by chemical cleavage. Many chemical triggers have been applied as reduction of disulfide bonds, the cleavage of the acetyl groups by acids and the cleavage of peptides by enzymes, resulting in a faster release.[50]

Shell wall depolimerization: The method triggers the depolymerization of the shell, through the interaction with enzymes, light, acid and base,[50] releasing the active substance.

2. 3 Surface Plasmon Resonance (SPR) in nanoparticles

Metallic nanoparticles are characterized by a surface plasmon resonance (SPR), figure 2.2. This phenomenon involves the collective (resonant) oscillation of conduction electrons, when perturbed (for instance, by a specific wavelength), and allows to the nanoparticles to scatter (image) and/or absorb (heat) light.[16, 51 - 52] This effect is a fundamental concept for designing smart nanomaterials (polymeric structures, bio/molecules or host), once it allows to activate their mechanism of action.[35, 51] These nanomaterials can be configured in different shapes, sizes, structures, composition and dielectric medium according to the applications.[51]

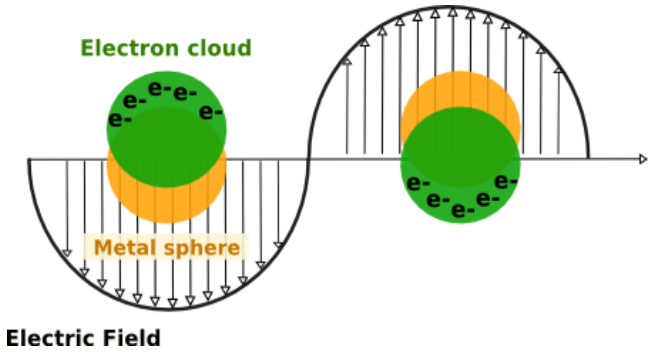

Figure 2.2 - Schematic representation of surface plasmon oscillation of metallic nanoparticles.

Source: By the author.

Silver nanoparticles have interesting properties in plasmonics from antibacterial to nanoantennas applications.[53 - 54] In plasmonics, silver nanostructures can respond in the wavelength range from 300 to 1200 nm.[55] Besides, the surface plasmon is dependent on its dielectric function ε, which include a real part (ε_r) and an imaginary part (ε_i), and both can vary to a determined wavelength (λ).[56] A simple way to represent localized SPR (LSPR) can be found in Mie theory.[57] For calculation of the extinction (absorption + scattering) cross section of a metal nanoparticle:

$$C_{ext} = \frac{24\pi^2 R^3 \varepsilon_m^{3/2}}{\lambda}\left[\frac{\varepsilon_i}{(\varepsilon_r + 2\varepsilon_m)^2 + \varepsilon_i^2}\right] \quad (2.1)$$

Where C_{ext} is the extinction cross-section, R is the radius, and ε_m is the relative dielectric constant of the medium surrounding the nanoparticle.[56] This equation shows that the dielectric properties (ε_r and ε_i) give the way of interaction between nanomaterial and light. Even though, others parameters are fixed as plasmonic characteristics and excitation wavelength.[56] When the denominator of the bracketed expression in the equation 2.1 approaches to zero, C_{ext} will become large and the optical absorption and scattering at this frequency will also be strong. This is known as a resonance condition.[56]

2. 4 Antibacterial properties of silver nanoparticles

AgNps serve as a vehicle to deliver Ag^+ more effectively to the bacterial cytoplasm and membrane for antibacterial applications.[58] The release of silver ions from crystalline core of nanoparticles promotes the generation of disequilibrium inside of the cell,[59] as depicted in figure 2.3. Silver cation targets and binds to negatively charged components of proteins and nucleic acids, thereby causing structural changes and deformations in bacterial cell walls, membranes, and nucleic acids.[60 - 61] In fact, silver ions are generally known to interact with electron donor functional groups like thiols, phosphates, hydroxyls, imidazoles, indoles, and amines.[62] Accordingly, it is believed that silver ions bind to DNA block transcription and cell surface components, which interrupt bacterial respiration and adenosinetriphosphate (ATP) synthesis.[63 - 64] Other reports suggest that silver ions block the respiratory chain of microorganisms in the cytochrome oxidase and nicotinamide adenine dinueocleotide (NADH)-succinatedehydrogenase region, being an enzyme complex in bacterial cells.[65]

Additionally, some reports have mentioned the inhibition of oxidation of succinate, glycerol, glucose, and other molecules in *E. coli* due to silver ions.[62] AgNps of smaller sizes contribute with a higher antibacterial activity, due to their higher surface area associated to the faster Ag^+ release compared to large AgNps.[66] The environmental and biomedical impact could be mitigated by modulating Ag^+ release, possibly through manipulation of oxygen availability, particle size, shape and type of coating.[59]

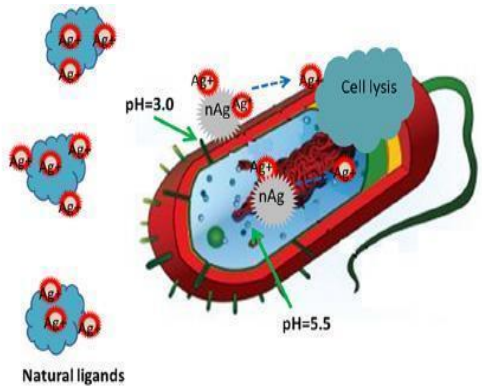

Figure 2.3 - Schematic representation of the interaction of silver nanoparticles with bacteria.

Source: XIU et al.[18]

2. 5 Chitosan and Aniline

Chitosan is a linear polysaccharide obtained by deacetylation of chitin moieties, with biodegradable and biocompatible characteristics, being soluble in organic acid when pH < 6, while its pKa is 6.2.[67] It is considered to have a good chelating ability, where the chelation is related to the $–NH_2$ content as well $–NH_2$ distribution,[68] as illustrated in figure 2.4.

Chitosan has shown interesting characteristics as biocompability, biodegrability, mucoadhesivity, and anti-infection ability.[67-68] The antimicrobial activity is due to the interactions between their positive charge and negative charge of microbial cell membrane.[69] This process leads to a leakage of intracellular constituents and alteration of cell

permeability.[68] However, studies have shown the ability of modulate the inflammatory responses in human fibroblast,[70] since, amino groups can be protonated and in the presence of proton ions that are released in the inflammatory area, resulting in a analgesic effect.[71]

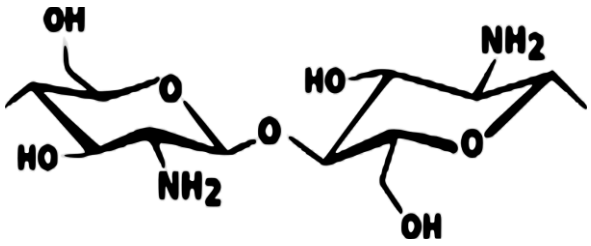

Figure 2.4 - Molecular representation of chitosan.

Source: By the author.

Aniline is an organic chemical compound, specifically a primary aromatic amine, consisting of a benzene ring attached to an amino group,[72] as depicted in Figure 2.5. Aniline has a boiling point at 184 ^{o}C, a melting point at -6 ^{o}C and pKa of 4.62.[72] It is an electroactive compound, with photoelectrocatalityc degradation[73]. The unshared electron pair on the aniline is delocalized and therefore less available to donate.[74] The antibacterial effects can be explained through electrostatic adherence between the aniline molecules and bacteria.[75]

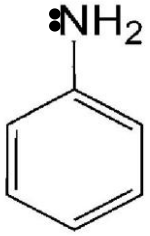

Figure 2.5 - Molecular representation of aniline.

Source: By the author.

2.6 Experimental

2.6.1 Materials

Chitosan (CS, medium molecular weight), Aniline Hydrochloride ≥ 99.0% (mw = 129.59 g/mol), Silver Nitrate (mw = 169.87 g/mol), Sodium Borohydrade granular, 99.99%

(mw = 33.83 g/mol) were purchased from Sigma-Aldrich. Glacial Acetic Acid (CH_3COOH) was purchased from Synth (Industria Brasilera, São Paulo, Brazil). All aqueous solutions were prepared with double-distilled water and the chemicals were used without further purification.

2.6.2 Synthesis of AgNps-Nanocapsules using a complexation-reduction method

The synthesis of the AgNps-nanocapsules was carried out through a complexation-reduction method adapted from a previous work reported by Fwu-Long Mi et al[76]. Initially, chitosan (CS)(16,5 % w/v, 50 mL) was dissolved in acetic acid (1 % v/v, 50 mL), then Aniline (A) hydrochloride (10 mM) were mixed with the CS solution and left under magnetic stirring for 1 h. The reaction produces cross-linking between aniline and chitosan due to the covalent character between the two molecules.[77 - 80] After this procedure, $AgNO_3$ (0.5 mM) was added to the solution (chitosan-aniline) and mixed by 1 h under magnetic stirring, until the resulting mixture appeared milky with greenish opalescence. Silver ions in the A-CS complex were reduced by using $NaBH_4$ (4.5 mM) in a controlled procedure at room temperature. Specifically, $NaBH_4$ (100 mL) was added to the solution at intervals of 30 min (three times) in order to protonate the NH_2 group in aniline (A) to NH_3^+ and to enhance the hydrogen bonds to $-OH^-$ groups of chitosan (CS). Silver ions in the A-CS complex nanocapsule chelate in AgNps, because the protonated amine ($-NH_3^+$) of CS inside the nanocapsule attracts the ions and permits the formation of AgNps,[76] as illustrated in figure 2.7. The synthesized material was washed by centrifugation first for 2 min to 10000 g to eliminate residues of the synthesis and a second time by 1min, 10000 g.

(a)

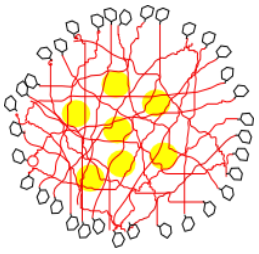

continue

continuation

(b)

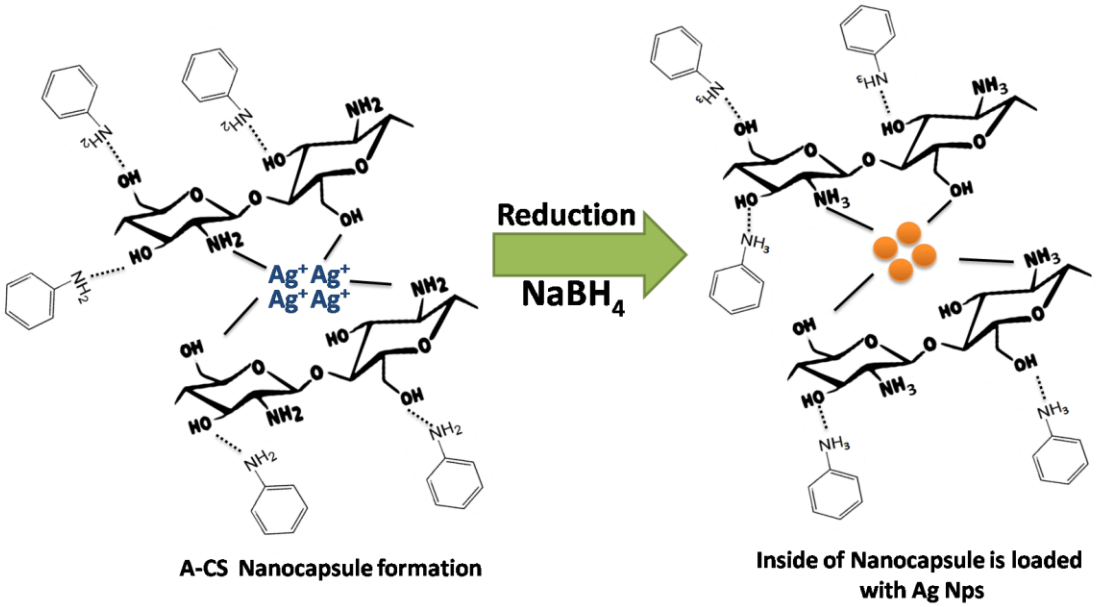

Figure 2.6 - The linkage between protonated amine groups of aniline (A) and chitosan (CS) and OH^- of CS form the nanocapsules. The inside of the nanocapsule is loaded with AgNps which is stabilized by protonated amine groups of CS (a) Schematic design of AgNps-Nanocapsule, (b) Schematic diagram of preparation of A-CS Nanocapsule loaded with AgNps.

Source: Adapted from FWU-LONG MI et al.[76]

2.6.3 Determination of concentration of AgNps – Nanocapsules

To determine the concentration of AgNps – Nanocapsules 1 mL of dispersion was poured on glass sheets (triplicate). The dispersion of AgNps – Nanocapsules was then dried using a vacuum pump (TBV5-Tander). At the end of drying process, the concentration of nanocapsule was determined in 57.6µg/mL.

2.6.4 Characterization Techniques

UV-Vis absorption was used to detect the optical properties of the nanosystem. The measurements were recorded from 200 to 700 nm at room temperature (Hitachi U-2900 spectrophotometer). The Morphology studies of nanomaterials (nanofibers, nanocapsules and nanoparticles) were carried out using a field emission scanning electron microscopy (FESEM)

(JEOL-JSM 6701F), with the nanomaterials diameter being estimated with image analysis software (ImageJ, National Institutes of Health, USA). The dynamic light scattering (DLS) and Zeta Potential (ξ) experiments were conducted using a Zetatrac from Microtrac Inc, to determine the size and charge of the Ag Nps-nanocapsules and their components. Fourier transform infrared spectroscopy (FT-IR) was used to understand the attachment between the functional groups of CS and A in the Ag Nps-nanocapsule and their components. Measurements were performed on silicon wafers with a Nicolet 6700 FT-IR.

2.6.5 Synthesis of Ag-Chitosan Nanoparticles (AgNps-CS)

AgNps-CS nanoparticles were prepared to compare their properties with AgNps-nanocapsules. For preparing the AgNps-CS nanoparticles, CS (16.5% w/v) was dissolved in acetic acid (1 % v/v, 25 mL). Then, $AgNO_3$ (0.5 mM) was added to the solution, which was kept at room temperature for 10 min.[81] Subsequently, the reducing agent $NaBH_4$ (4.5 mM, 100mL) was added and the solution was kept under magnetic stirring during 1 h.[81] One drop of the dispersion of AgNps-CS were poured on silicon sheet and dried using vacuum pump without any type of coating for the field-emission scanning electron microscopy (FESEM) micrographs. The Figure 2.7 shows the FESEM images of AgNps-CS nanoparticles, with average size of 17±3 nm.

Figure 2.7 – FESEM images of silver nanoparticles coated by chitosan with size of 17±3 nm.Which it is used to compare in the characterization with the AgNps-Nanocapsule.

Source: By the author.

2.7 Results and discussion

The morphology of AgNps-nanocapsules is shown by FESEM image in Figure 2.8a. The nanocapsules have an average size of 78 ± 19 nm, value comparable to the size determined by dynamic light scattering (DLS) technique, showing an average diameter of 79 nm, with a polydispersity index (PdI) of 0.281 (monodispersive distribution), Figure 2.8b. The Zeta potential was found at +39 mV.

In figure 2.8a, it is observed the AgNps in the chitosan-aniline nanocapsule. This nanostructure can be classified as a nanogel structure[45], once the nanocapsule formation is produced by the cross-linked between chitosan and aniline interaction,[77 - 80] while the AgNps is localized inside the polymeric network. The size of AgNps inside the nanocapsule was estimated (using ImageJ software) as 18 ± 3 nm.

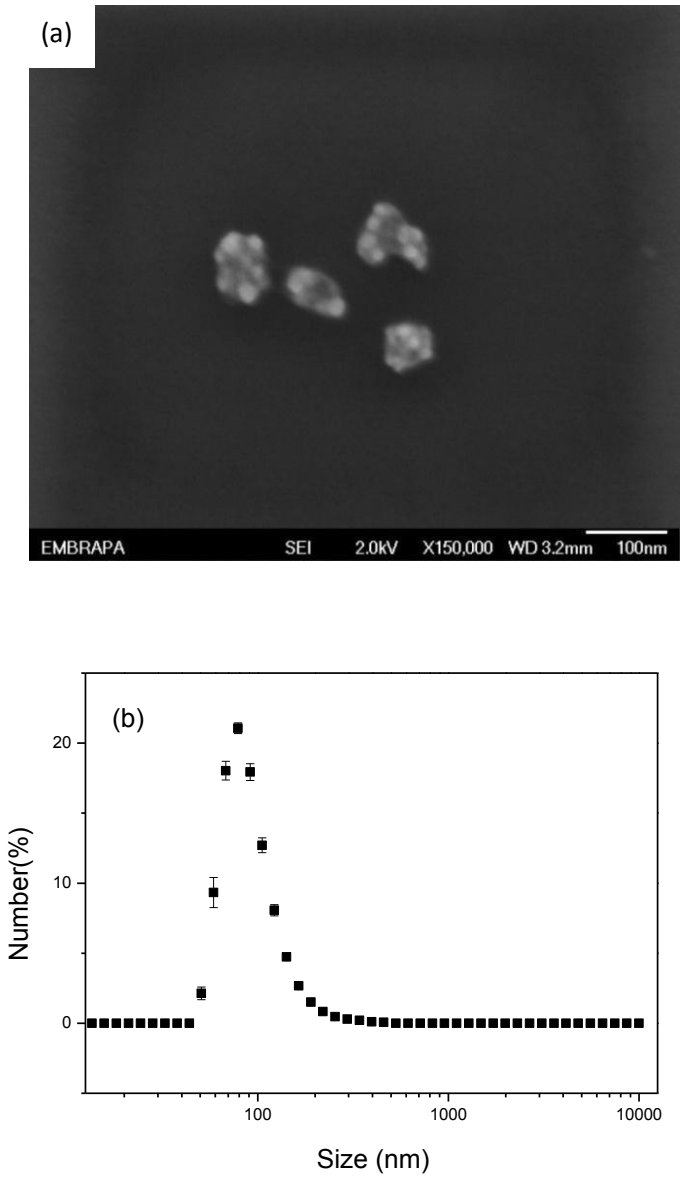

Figure 2.8 - a) FESEM images of AgNps-nanocapsules with average size of 78 ± 19 nm, (b) DLS of AgNps-nanocapsules in pH 7.2 with a size distribution of 79 nm and PdI 0.281. The Zeta potential was found at +39 mV. The nanoparticle size inside of nanocapsule was determined by ImageJ software with an averege size of 18±3 nm.

Source: By the author.

The UV-Vis absorbance spectrum of the AgNps-nanocapsules shows a surface plasmon resonance (SPR) of AgNps at 405 nm. A single band observed at 270 nm (Figure 2.9) is due to the π-π^* transition of benzene rings and excitation of the quinoid rings of aniline.[82]

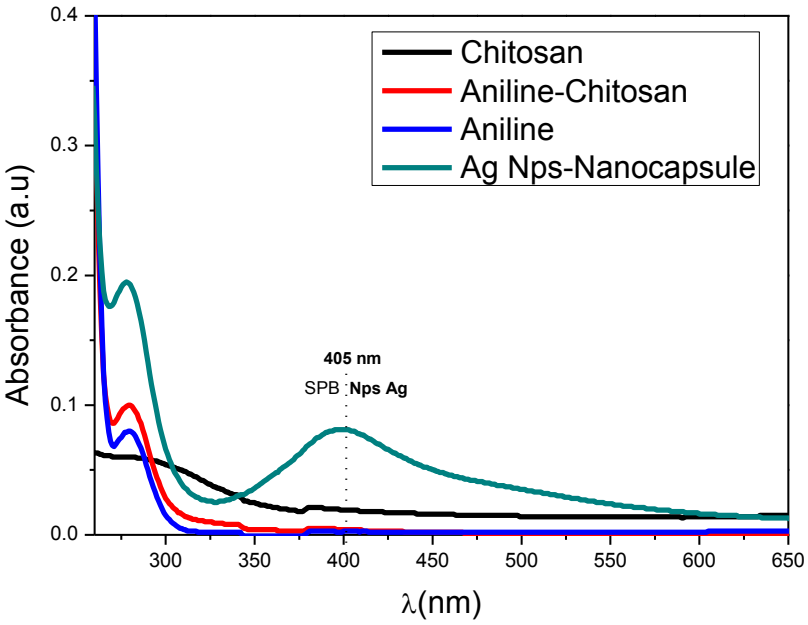

Figure 2.9 - UV-Vis absorption spectra of the Ag Np-Nanocapsule, displaying the surface plasmon resonance (SPR) at 405 nm, while the band at 270 nm originates from the π-π^* transition of benzene rings.

Source: By the author.

The characteristic surface plasmon absorption band of AgNps-nanocapsule reveals the presence of AgNps inside the nanocapsules. The nanocapsule formation originated from the cross-linking between the $-NH_3^+$ protonated groups of aniline and OH^- groups of CS.[77 - 78] The solubilization of CS in acetic acid solution results in an increase in the protonation level of CS.[83] The protonated amine group ($-NH_3^+$) in CS causes electrostatic repulsion and act as a chelating agent that forces the silver ions to chelate and form AgNps inside of the nanocapsule, as illustrated in figure 2.8.

Nanocapsules without AgNps were produced using the same proportion of chitosan and aniline and the same concentration of reducing agent, yielding to nanocapsules with larger size and wider size distribution, 0.74 ± 0.26 µm, as displayed in FESEM images of Figure 2.10. The protonated amine $-NH_3^+$ of CS inside the nanocapsule generates charge repulsion between them, once it does not have Ag^+ to chelate, therefore leading to different charge distributions and different nanocapsule sizes.

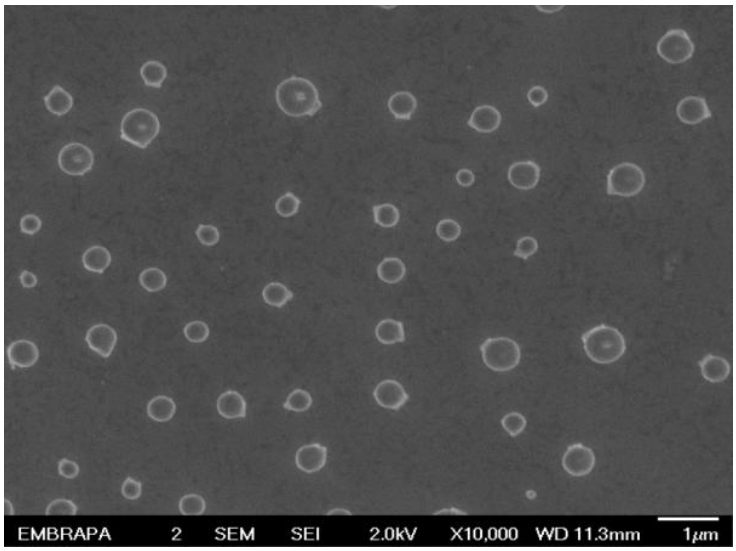

Figure 2.10 – FESEM image of Nanocapsule in the absence of AgNps. Different sizes of nanocapsules are caused by strong electrostatic repulsion between NH^{3+} groups of CS inside of the nanocapsules when there are not AgNps.

Source: By the author.

The average size of AgNps-nanocapsules as a function of pH and their stability as a function of time (pH = 3 and 7) was investigated, as illustrated in figure 2.11a, b and c, respectively. Changes in pH modify the molecular conformation; for instance, the nanocapsules are stable from pH 3 to pH 7.5, once the protonated amine groups in A attach to the hydroxyl groups of CS, leading the formation of nanocapsules. On the other hand, in alkaline pH, the interactions between functional groups of CS and A are affected by deprotonation of amine groups, which changes the morphological conformation of AgNps-nanocapsules, leading to aggregation, figure 2.11a.

The stability of the AgNps-nanocapsules was also observed during a period of 10 days with measurements at each 12 h. The measures were collected for AgNps-nanocapsules dispersion at pH 3 and pH 7 by DLS. The nanocapsules were determined stable at 10 days, since from day 10 at pH 7 was observed a change of size distribution and for pH 3 was reported a variation of PdI greater than 0.5, in both cases there are an increase of polydispersivity of the system,[84 - 86] figure 2.11b and c.

(a)

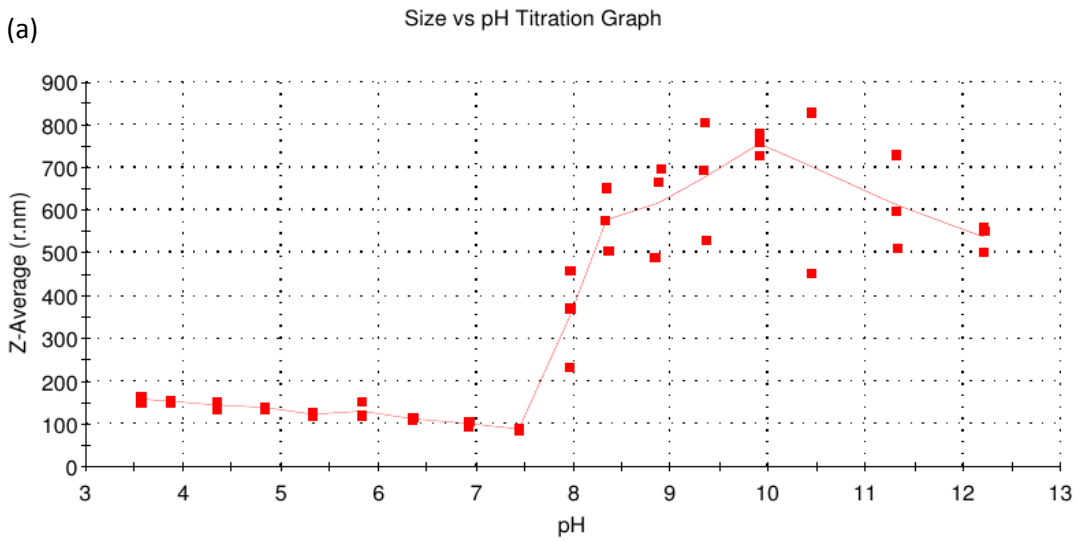
Size vs pH Titration Graph
Z-Average (r.nm)
pH
0
100
200
300
400
500
600
700
800
900
3
4
5
6
7
8
9
10
11
12
13

(b)

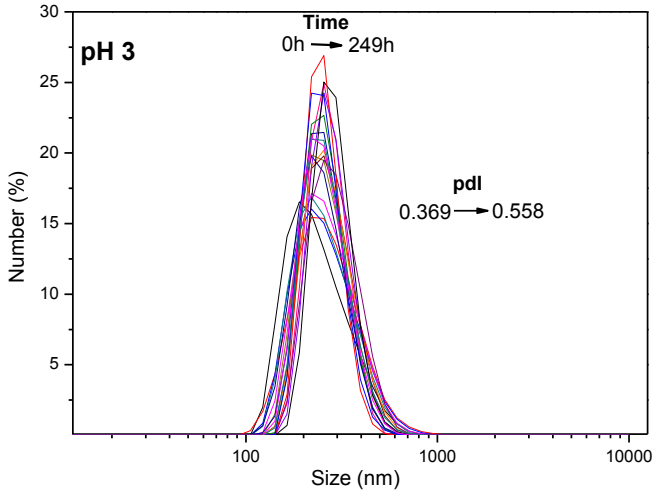
pH 3
Time
0h → 249h
pdl
0.369 → 0.558
Number (%)
Size (nm)
5
10
15
20
25
30
100
1000
10000

continue

continuation

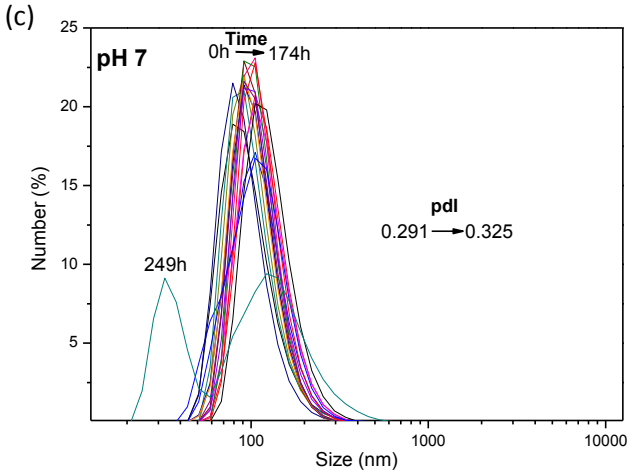

Figure 2.11 – Average size of AgNps-nanocapsules as a function of pH. The nanocapsule system is stable from acid to physiological pH. In alkaline pH, AgNps-nanocapsules start to aggregate due to the deprotonation of amino groups in CS and Aniline (a). The stability of AgNps-Nanocapsules as a function of time in pH 3 and pH 7 (data collected by DLS) (b) and (c).

Source: By the author.

FT-IR spectra were collected in order to elucidate the interactions between the functional groups of the AgNps-Nanocapsules components. The interaction between protonated amines and hydroxyl groups of the A-CS was verified in the nanocapsule formation. The development of AgNps inside the nanocapsules was observed in the protonated amine group of CS. The result is compared to the AgNps-Chitosan nanoparticles (AgNps-CS) on FT-IR spectra, shown in the figure 2.12.

The FT-IR spectra of AgNps-CS and CS are shown in Figure 2.12 (a) and (b). The bands at 1381, 1334 and 654 cm^{-1} in Figure 2.12a correspond to the stretching groups –C-H- and -N-H- in CS after silver ions chelation.[87 - 88] Figure 2.12c and 2.12d demonstrate the cross-linking of A-CS in the formation of nanocapsules.[78 - 80] The bands at 3349, 2810, 2599 and 2025 cm^{-1} are found both in the CS and the aniline FT-IR spectra. This behavior could indicate that many hydrogen bonds are formed between the protonated amine –N-H- of CS and A, and O-H- of CS. The two bands at 1591 and 1497 cm^{-1} for AgNps-nanocapsules (Figure 2.12d) are assigned to the quinoid ring and benzene ring of A which can be compared to A in Figure 2.12c.[84]

In Figure 2.13a, the FTIR spectra of AgNps-nanocapsule and AgNps-CS are displayed. It is observed a deformation and stretching at 1392 cm^{-1} that corresponding to protonated amine –N-H- in CS after those chelate silver ions to form AgNps inside of the nanocapsule.[49, 87, 89]

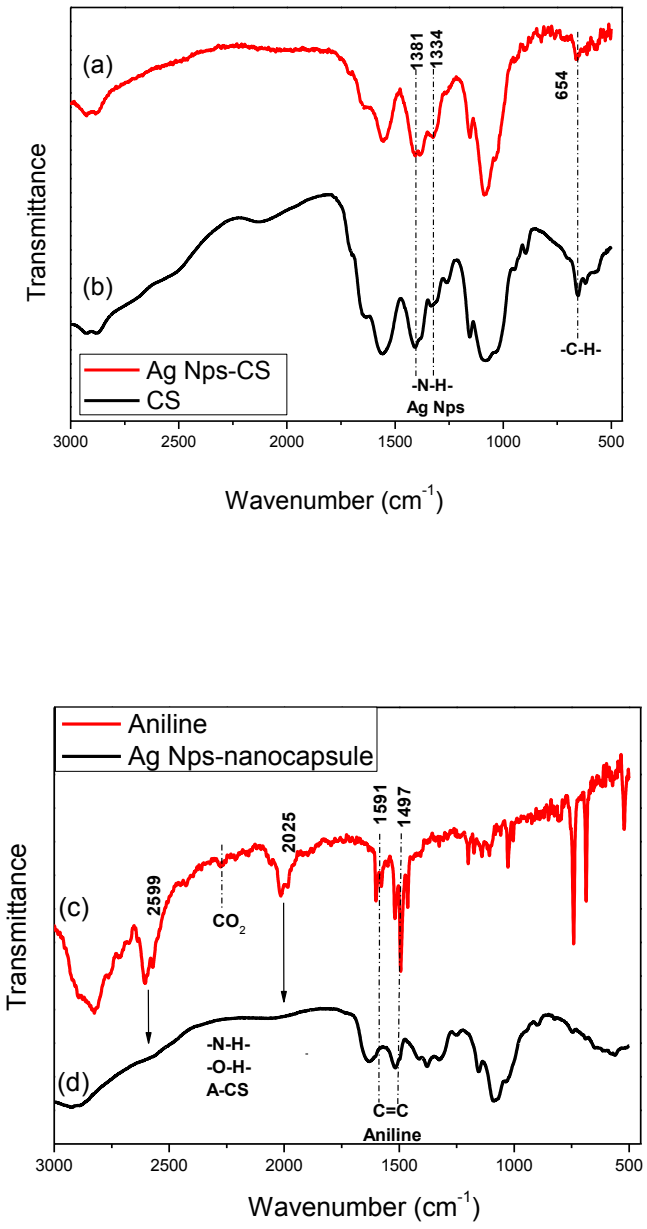

Figure 2.12 - FT-IR spectra show the interaction between functional groups in the formation of nanocapsules and AgNps: (a) AgNps-CS, (b) CS, (c) Aniline, (d) AgNps-nanocapsules.

Source: By the author.

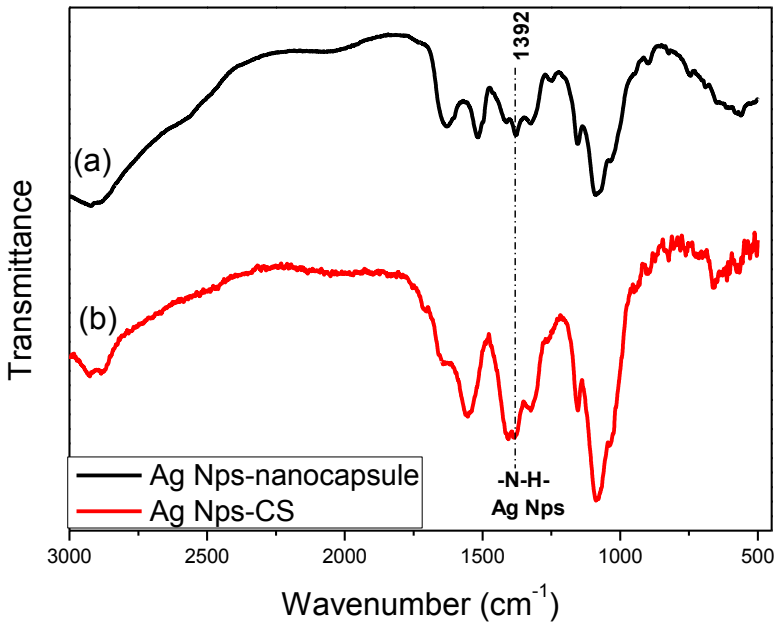

Figure 2.13 - FT-IR spectra shows the formation of AgNps after chelation inside polymeric network of CS in both cases (a) AgNps-nanocapsules and (b) AgNps-CS.

Source: By the author.

2.8 Synthesis and characterization of electrospun Nanofibers

2.8.1 Polycaprolactone

Polycaprolactone (PCL) $(C_6H_{10}O_2)_n$ is a poly(α-ester) of aliphatic ester linkages, hydrolitically unstable, which chemical structure is displayed in figure 2.14. The physical, mechanical, chemical and thermal properties of PCL are dependent on their molecular weight and crystanillity grade.[90] At room temperature, PCL is highly soluble in chloroform, dichloromethane, N,N-dimethylformamide, cyclohexane, carbon tetrachloride, benzene, toluene, lightly soluble on acetone, ethyl acetate and insoluble in alcohols, diethyl ether and water.[91]

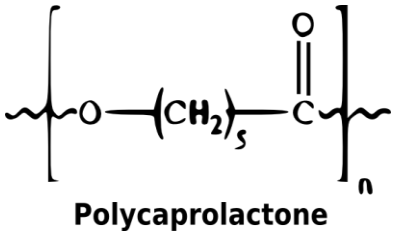

Figure 2.14 – Chemical structure of polycaprolactone.

Source: By the author.

The degradation time of PCL depends on the molecular weight, crystanillity level and the environmental conditions. The PCL can undergo hydrolytic and enzymatic degradation, which are self-catalyzed by carboxylate acids released during the reactions. Several studies have shown that PCL is not toxic and displays cytocompatibility with different body tissues.[91] In addition, their surface can be modified from originally hydrophobic to hydrophilic by physics methods, including oxygen plasma, which makes possible the surface functionalization with hydrophilic polymers for biomedical applications.

PCL nanofibers (PCL Nfs) produced by electrospining exhibit morphological properties analogues as the protein structures of extracellular matrix.[92] This property is interesting as biomimetic medium in adhesion, proliferation, migration cell, as well as in biofilm expressed by bacteria. In spite of these properties, the PCL Nfs does not have bioactivity characteristics, which can be achieved by the modification of their surface with bio-nanomaterials.[93]

2.8.2 Electrospining technique

The electrospinning technique uses an electric potential to eject a polymer solution drop located at the tip of a needle until a metallic collector, as illustrated in figure 2.15. Basically, the polymeric solution drop is kept at the needle tip due the superficial tension. By applying an electrical field, the repulsion charge in the solution generates a force directly opposed to the surface force acting on the solution drop.[94] The increasing of the electric potential produce an elongation of the drop, in a conic form, which is called Taylor cone.[95] When the electrostatic repulsion forces overcome the surface tension force acting on the drop, a jet is expelled from the cone. The jet electrically charged gradually loses volume in the air

due to the elongation of the fiber and the solvent evaporation[96] while is directed to the collector.

The synthesis of nanofibers by electrospining depends of several parameters. Polymer and solution parameters, such as molecular weight and distribution, viscosity, surface tension and conductivity, influence the nanofiber diameter and the presence of surface defects (as beads).[97- 98] The parameters of the process, including diameter of needle, flow rate of polymer, electrical potential, distance between the needle and collector influences the morphology of nanofibers, and the evaporation of the solvent. Several configurations of setups and collectors for the nanofiber deposition can be employed.[97- 98]

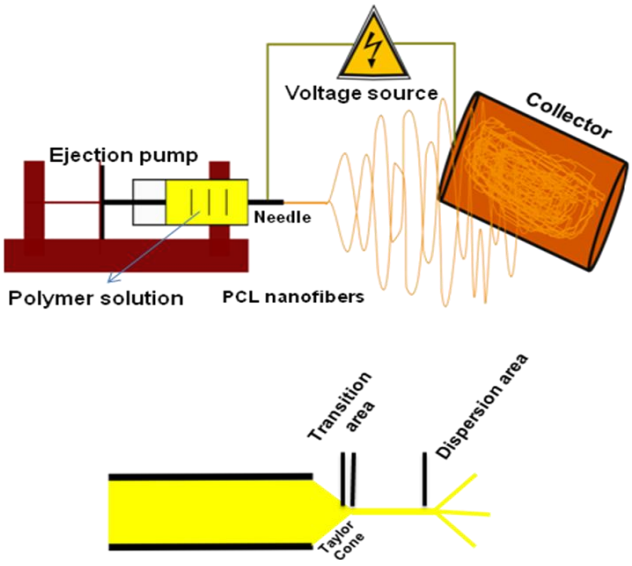

Figure 2.15 - Schematic representation of electrospining technique and their components.

Source: By the author.

2.9 Experimental

2.9.1 Materials

N,N-dimethylformamide (DMF), dichloromethane (DCM), silver nitrate ($AgNO_3$) and polycaprolactone (PCL) (MN= 80.000) were purchased from Sigma-Aldrich.

2.9.2 Fabrication Ag Nanoparticles embedded in PCL nanofibers

For the fabrication of polycaprolactone nanofibers, PCL (8% wt/v) was mixed with dichloromethane (DCM) and N,N-dimethylformamide, (3:7 v/v) and left under magnetic stirring for 5 h, until total dissolution was achieved, yielding a solution viscosity of 80.7 cP.

For the fabrication of AgNps embedded in the bulk of polycaprolactone nanofibers, N,N-dimethylformamide (DMF) was used as a slowly reducing agent for silver ions.[99] Initially, 20 mM of $AgNO_3$ were dissolved in DMF and the formation of the silver nanoparticles was manifested with the yellowish coloration in the dispersion. AgNps-DMF was mixed with dichloromethane (DCM), in the same proportion of polycaprolactone nanofibers (3:7, dichloromethane : AgNps-DMF) to which 8% wt/v of PCL pellets was added and left under magnetic stirring for 5 h, until total dissolution was achieved, yielding a solution a viscosity of 100,2 cP. All stages were carried out at room temperature.

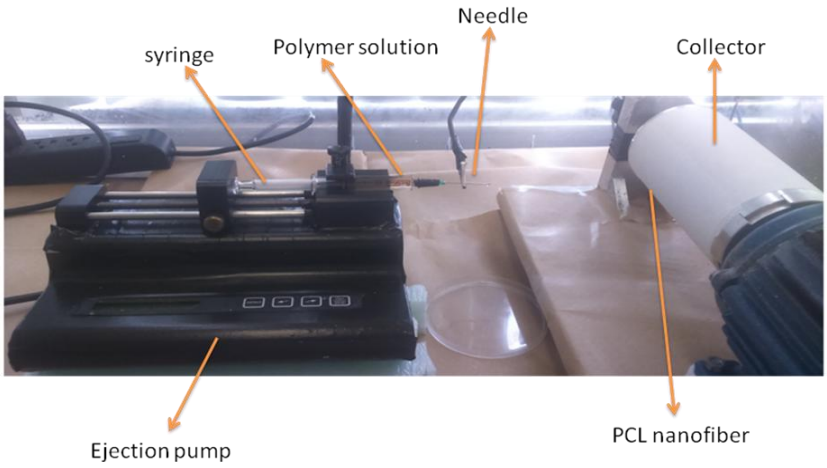

Figure 2.16 - Electrospining tecnhinique of Embrapa Instrumentation.

Source: By the author.

The electrospun nanofibers were obtained using an electrospinning apparatus available at Embrapa instrumentation, using a feed rate of 0.5 mL/h and electric voltage of 17 kV. A picture of the apparatus is displayed in figure 2.16. A working distance of 12 cm was kept between syringe and the metallic collector. The inner diameter of the steel needle was of 0.7 mm. Nanofibers were directly deposited onto the aluminum foil wrapped around the collector,

using a rotation speed of 150 rpm and a collection time of 1h. Control of the experimental conditions was important to ensure reproducibility, once the diameter and morphology of nanofibers depend on all parameters associated to electrospinning.

The morphology of the nanofibers was analyzed using a scanning electronic microscope (FESEM) model JEOL 6510, for which the samples were covered with carbon powder. In order to determine the average diameter and their distribution, 100 random nanofibers were analyzed using the software of image, Image J of National Institutes of Health, USA.

2.10 Results and discussion

PCL nanofibers were electrospun with diameter of 240 ± 70nm, and presented homogeneous morphology without porosity, superficial deffects and imperfection (beads) as displayed in FESEM image in figure 2.17. The homogeneous morphology of the nanofibers can be explained by the correct choice of the experimental parameters and stability of polymeric solution along the stretching during nanofiber formation before reaching the collector.

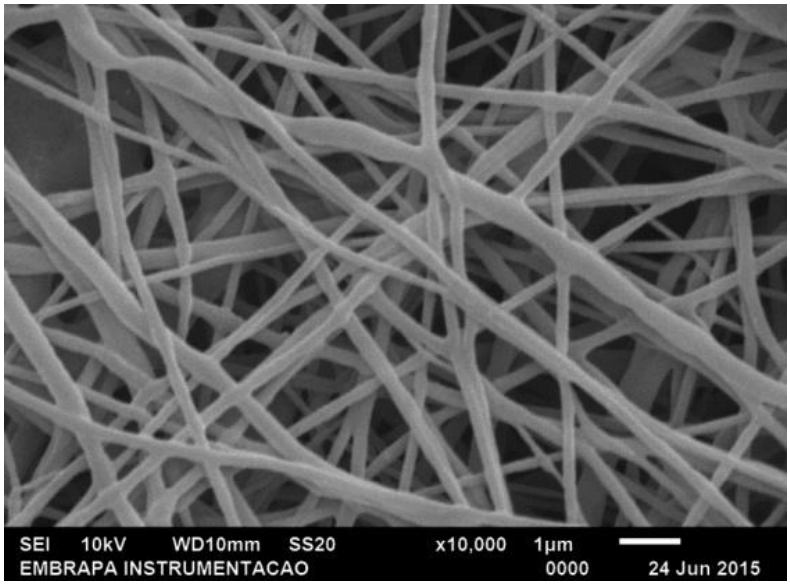

Figure 2.17 - FESEM image of NFs PCL morphology.

Source: By the author.

The PCL nanofibers containing AgNps were produced using the same conditions employed for the fabrication of net PCL nanofibers, and the silver ions were reduced to metallic silver by N,N-dimethylformamide (DMF). A proportion of 3:7 between dichloromethane and AgNps stabilized in dimethylformamide (DCM:AgNpsDMF) was employed. AgNps can be observed along the bulk of PCL nanofiber, according to FESEM images displayed in figure 2.18, whose nanofibers show homogenous morphology, without porosity and beads. The AgNps appear brighter than the nanofibers due to their higher electronic density. An increment in the diameter of PCL nanofibers containing AgNps (417 ± 14) nm is observed due to the increase of solution conductivity caused by the AgNps.

The formation of silver nanoparticles into the nanofiber bulk avoids their direct contact with the surrounding environment or host. This characteristic is important, once it can decrease possible toxic effects of AgNPs to the host, while the mechanism of action is based on the release of silver ions from the nanofiber bulk, which principle is discussed in the next chapter.

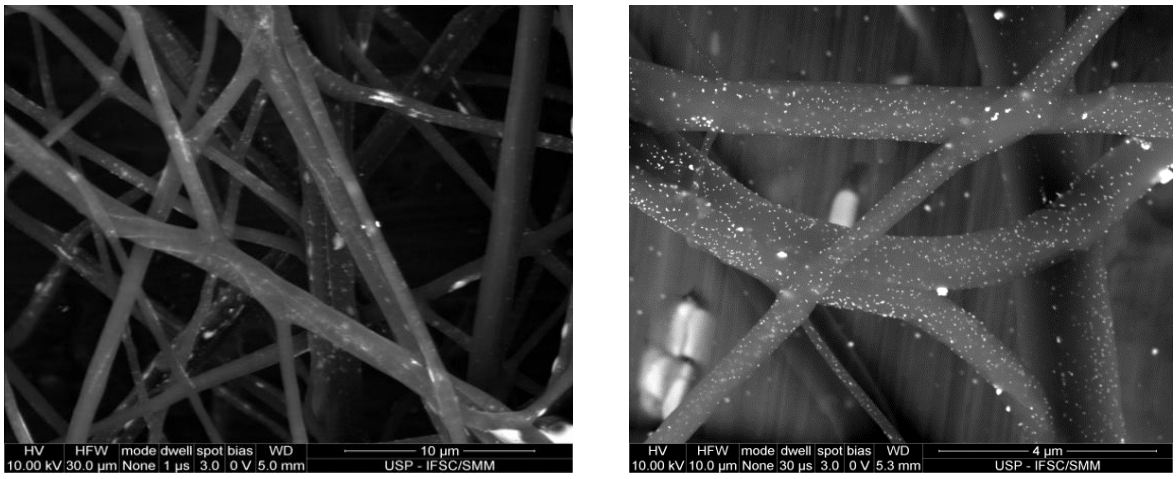

Figure 2.18 – FESEM image by backscattering electrons scan shows the difference of contrast between AgNps and PCL nanofibers

Source: By the author.

The surface of AgNps-PCL nanofibers was modified by means of oxygen plasma treatment. The nanofibers mats were submitted to this treatment during 2 min (5 % W) to increase their hydrophilicity, breaking the ester bonds and producing carboxylate functional groups. Figure 2.19 shows the image of contact angle measurements regarding the deposition

of water drop on the PCL nanofibers and plasma-modified PCL nanofibers.[100] The contact angles were 90.4 ± 3.8˚ for PCL nanofiber and 57.7± 3.8˚ for plasma-modified PCL nanofiber.

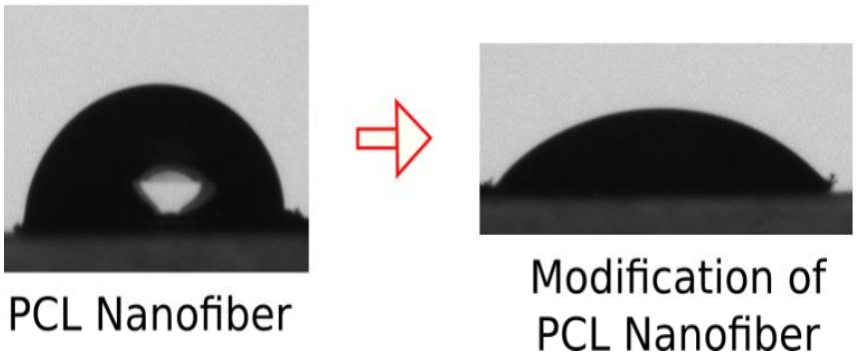

Figure 2.19 - Surface modification of PCL nanofibers by oxygen plasma during 2 min at 5 W. Images of contact angle before and after the modification.

Source: By the author.

2.7 Conclusion

We presented the synthesis and characterizations of the AgNps-Nanocapsule. The AgNps were chelated in the aniline-chitosan nanocapsular configuration, which cross-linking occurred between protonated amine groups of aniline and chitosan and OH^- of chitosan.[80] The presence of AgNps was confirmed by UV-Vis absorption spectrum, with a surface plasmon band at 405 nm as well by scanning electron microscopy. The average size of the AgNps-nanocapsule was 78.1 ± 19.2 nm with a monodispersive distribution. This nanocapsule can be considered as a nanogel structure, where their formation is caused by the cross-linked between chitosan and aniline. The AgNps are localized inside of the polymeric network of chitosan. This nanomaterial has a SPR band that can be stimulated by light at 405 nm. Upon irradiation an increase in the kinetic energy of the system occurs, generating detachment of AgNps from the polymeric network. This characteristic can be interesting for antibacterial application.

PCL nanofibers containing AgNps were fabricated by the electrospinning technique with good homogeneity and stability. The morphology is optimal for antibacterial application

since they have a similar structure to proteins expressed by biofilm forming bacteria. After nanofibers fabrication, their surface was modified with oxygen plasma to change its hydrophobicity. Such procedure allows the functionalization of nanofiber mats with the AgNps-Nanocapsules, forming a smart nanosystem. This smart nanomaterial can be used as an antibacterial system activated by light.

3 Photoactivated AgNPs-nanofibers for antibacterial applications

3.1 Antibacterial nanofibers

Electrospining technology enables the fabrication of nanofibers with specific physico-chemistry properties and high area-to-volume ratio,[25] which allows the assembling and releasing of bio/materials as proteins, drugs, nanoparticles and nucleic acids. Also, these materials can be incorporated into nanofibers bulk or surface, improving the release for antibacterial, therapeutic or anti-inflammatory purposes.[25, 101]

The antibacterial nanofibers mats can be fabricated using hybrid nanomaterials, such as a synthetic or natural polymers in conjugation with the active substance.[102] For instance, polyurethane nanofibers containing silver nanoparticles,[25] which shown bactericidal properties for *E. Coli* and *S. tuphimurium* have already been reported, which system was capable of avoiding bacteria growth. Ascorbyl palmitate (AP), which is an amphipathic derivative of vitamin C capable of penetrating the skin and protect lipids from free radical peroxidation, has been used in conjugation with nanofibers and silver nanoparticles[103] for producing a material with antibacterial characteristics.[103] Other nanofibers systems composed by PAN/Ag_2CO_3 display a highly photocatalytic activity toward the degradation of methyl red dye solution under visible light.[104] In addition, PAN/Ag_2CO_3 composite NFs exhibit an antibacterial activity over *E. coli* and *S. aureus* under visible light due to photogenerated electron–hole pairs.[104]

3.2 Antibacterial application triggered by light irradiation

Approximately 1.7 million of patients are affected every year in the United States by infection[105], and therefore antibacterial therapies are in high demand in order to struggle the problems associated to these infections.[106] For this purpose, the antibacterial properties of visible light have been investigated, known as visible light therapy (VLT).[105, 107] Some of the VLT employs wavelengths at 405 nm to treat infection caused by several types of bacteria,

and it has been demonstrated to reduce bacterial growth using different intensities of light,[108 - 110] including B-lactam-resistant *E. coli*.[107] Moreover, light therapy can be combined with others nanomaterials to generate a synergic effect in the control of bacteria proliferation.[106] For example, laser irradiation at 632.8 nm has been employed on the release of flavonoid compounds from PEG-PLGA-gold nanoparticles, as a strategy for treatment of diseases.[111] Also, nanosystems based on gold core-silver shell nanorods were synthesized for bacterial control, where the plasmonic heating induced silver release. The presence of a silver shell substantially improved the antibacterial effect against both *S. epidermis* and *E.coli*[112] due to a synergistic effect between the materials.

3.3 Smart Nanomaterials activated by irradiation

Based on previous applications, our proposal is to assemble the PCL nanofibers with the AgNps-Nanocapsules to create an antibacterial system activated by laser irradiation at 405 nm, which can control the doses of silver ions released for antibacterial purposes, as illustrated in figure 3.1.

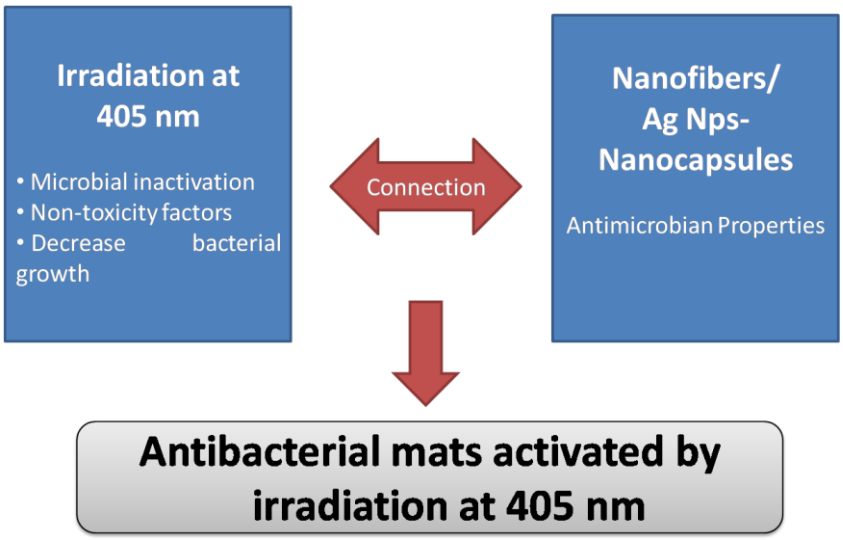

Figure 3.1 – Schematic representation of the assemble of PCL nanofibers with the AgNps-Nanocapsules to create an antibacterial nanofibers mat activated by laser irradiation at 405 nm.

Source: By the author.

3.4 Experimental

3.4.1 Kinetics of silver nanoparticle release

The study of photoactivated release of AgNps from the AgNps-Nanocapsule was carried out using a diode laser (DL5146-101S) at 405 nm with an intensity of 32 mW/cm^2, as illustrated in figure 3.2. For the measurements, 500 µL of nanocapsules dispersion (0.9 µg/mL) contained in a glass cuvette were irradiated at intervals of 30 s, during 600 s, changing the irradiated sample for every measurement, which were monitored by UV-Vis absorption spectroscopy (405 nm) at room temperature.

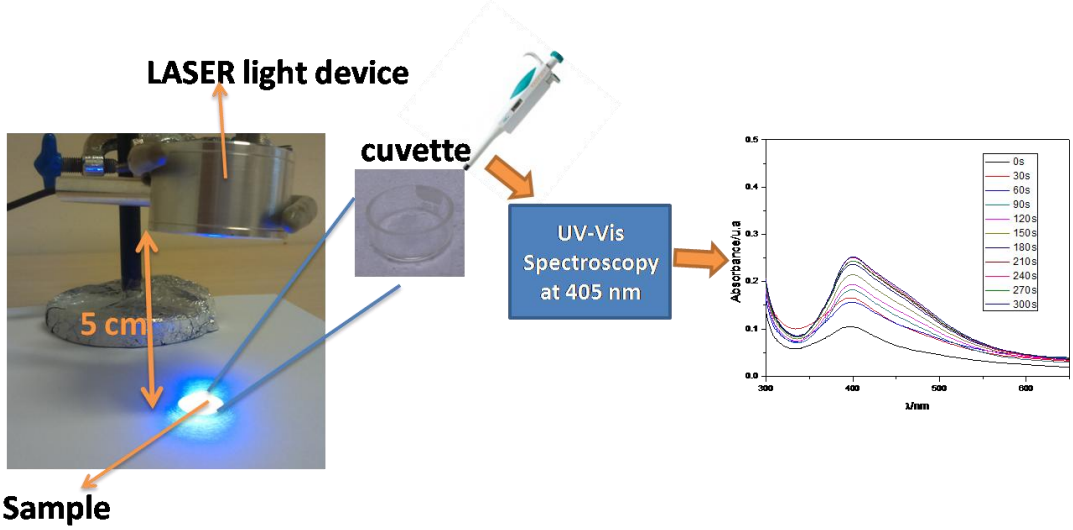

Figure 3.2 - Schematic representation of laser source used in the investigation of the release of Ag nanoparticles for antibacterial application and data collection.

Source: By the author.

3.4.2 Immobilization of AgNps-nanocapsules on PCL Nanofibers

The surface of PCL nanofibers were modified by means of oxygen plasma. The plasma was applied during 2 min (5 % W) on nanofibers mats, breaking the ester bonds and producing carboxylate functional groups.[101] AgNps-nanocapsules were immobilized on the

nanofiber surface by H-bonds and electrostatic interactions between the negative charge of nanofibers and amine functional groups of polymeric nanocapsules. Next, the nanofiber mats were immersed in a dispersion of AgNps-nanocapsules (57.6µg/mL), rinsed with distillated water and dried under ambient conditions. To determine the immobilization time of AgNps-nanocapsules on PCL nanofibers three immersion times (3, 7 and 10 min) were tested. The samples were visually inspected by FESEM microscopy and the time selected was 10 min, once it allowed a higher number of nanocapsules to be deposited onto the nanofiber surface compared to 3 and 7 min.

3.4.3 Bacteria

The antimicrobial activity of the developed system was evaluated against Gram-positive *Staphylococcus aureus* (ATCC 25923) and Gram-negative *Escherichia coli* (ATCC 25922) bacteria, using the facilities of microbiology laboratory of Embrapa instrumentation. The microorganism concentrations were adjusted to 1-5×10^6 cells/mL using 0.5 McFarland scale.

3.4.4 Agar diffusion method

The antimicrobial activity of the nanofiber mats was determined by the Agar diffusion technique according to the CLSI standard protocols 2009.[113] Agar was prepared in a solution of Mueller Hinton Broth and 30 mL was placed in each petri dish (150 mm of diameter). The nanofiber mats were cut into a disk shape having diameter of 2 cm. 100µl (1*10^6 cells/mL) of each microorganism *E. coli* and *S. aureus* were cultured on the agar and each disk were placed on it.

The laser source was placed 5 cm distant from the sample, which was irradiated for 150 s, according to the experiment of kinetics of silver nanoparticles release. After light exposure, agar dishes (triplicate) were incubated in an oven at 37 ˚C by 24 h.

3.5 Results and discussion

3.5.1 AgNps-nanocapsule Photoactivated by a laser source at 405 nm

AgNps-nanocapsules were irradiated with a laser source at 405 nm to excite the AgNps and produce their release from the nanocapsules, which was carried out through a kinetic study. The kinetics of release of Ag Nanoparticles was determined by UV-Vis absorption spectroscopy as described in section 3.2.1. After excitation, the AgNps plasmon band (405 nm) intensity increased, as illustrated in figure 3.3. The small red-shift for the SPR band is a result of the structural change in the polymeric nanocapsules (changes in the dielectric properties of the medium) after irradiation, while the increase in the intensity of the SPR band indicates that there is a disaggregation of the nanocapsules and release of AgNPs,[57, 114] Figure 3.3a. The time required to release the Ag Nanoparticles was determined as 150 s, according to Figure 3.3b. Dynamic light scattering shows the size distribution of the Ag nanoparticles after irradiation, with an average size of 18.17 nm and PdI of 0.479, as illustrated in Figure3.3c.

It is observed in figures 3.3 (a) and (b) that there is an initial absorbance different to zero, which increases as soon as the system is irradiated. This initial absorbance (t = 0s) is due to the silver nanoparticles exposed on the nanocapsules surface (figure 2.8a). After irradiation at 405 nm, the nanoparticles are detached or released due to excitation of the plasmon band that breaks the cross-linking of the nanocapsules, being complete at 150 s.

Comparing our system with other nanocapsules formed by cross-linking, it is reported the study of Kenichi Niikura et al,[115] who developed a polymeric nanocapsule composed of gold nanoparticles that due to the excitation of their SPR with laser irradiation at 532 nm, the cross-linking is broken and anti-cancer drugs are released.[115] In our case, the breakdown of cross-linking is given by the silver nanoparticles which are also the active substance.

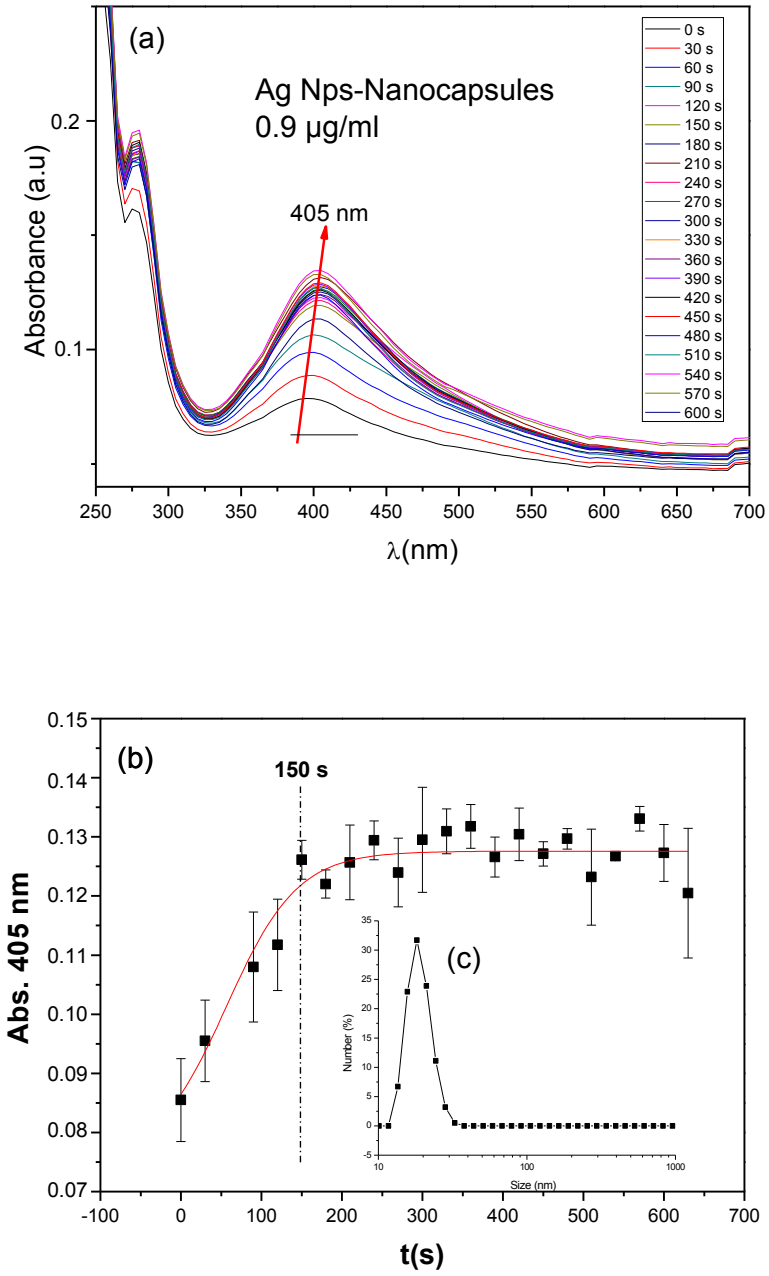

Figure 3.3 - Photoactivation of AgNps-Nanocapsules, (a) Kinetics of AgNps release through UV-Vis absorption spectra, (b) Release of Ag Nanoparticles as a function of time, monitoring the SPR band at 405 nm (c) DLS shows the size distribution of AgNps of 18.17 nm and PdI of 0.479 after irradiation.

Source: By the author.

3.5.2 Antibacterial mats activated by laser irradiation at 405 nm

3.5.2.1 Immobilization of AgNps-nanocapsules on PCL Nanofibers

AgNps-nanocapsules were expected to be immobilized on the nanofibers surface by H-bonds and electrostatic interactions between the negative charge of carboxylate functional groups of PCL nanofibers and amine functional groups of AgNps-nanocapsules. For that reason, the nanofiber mats were immersed in AgNps-nanocapsules dispersion as mentioned in section 3.4.2. The best adsorption time of the AgNps-nanocapsules on the nanofibers surface was optimized as 10 min. Figure 3.4 shows the FESEM images of nanofibers, which displays an uniform morphology and no beads. The average diameter of the nanofibers was estimated as 271 ± 85 nm.

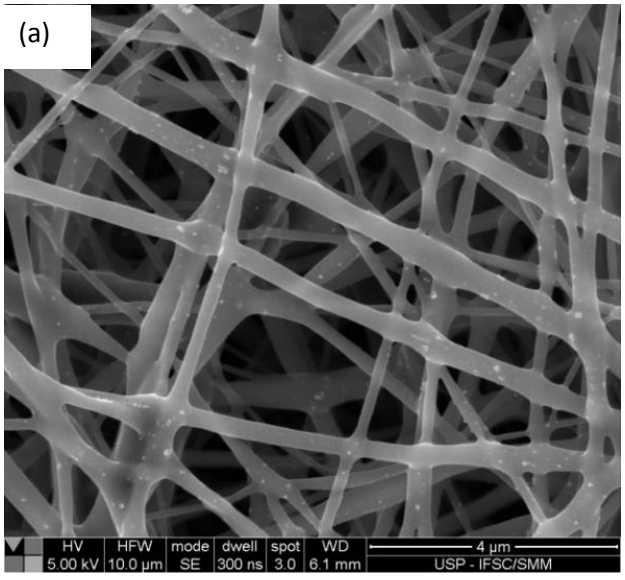

continue

Continuation

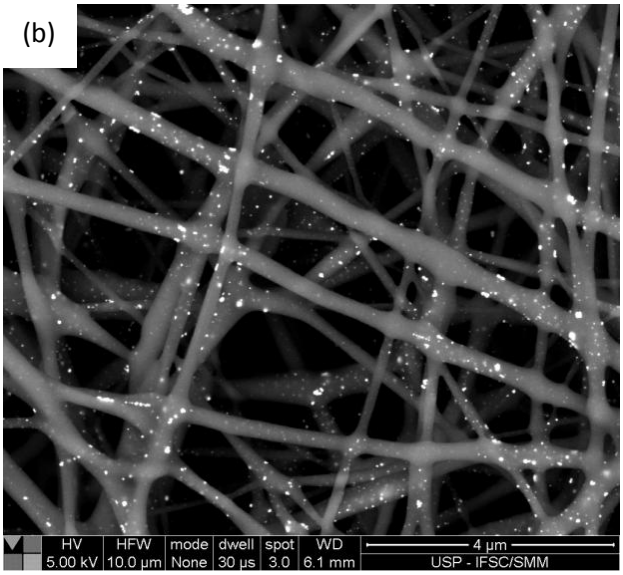

Figure 3.4 – FESEM image of PCL nanofibers functionalized with AgNps-nanocapsules. (a) secondary and (b) backscattering electrons show the difference between electronic density of AgNps-nanocapsules and PCL nanofiber.

Source: By the author.

Figure 3.4 shows the FESEM images collected using secondary electrons (Figure 3.4a) and backscattered electrons (Figure 3.4b), which shows the different electronic density of AgNps-Nanocapsules on PCL nanofibers.[116 - 117] The nanoparticles can be found on the surface and in the bulk of the PCL nanofibers, as expected by the method of preparation, according to the section 2.9.2.

The EDX spectrum shows the chemical composition of the nanosystem in a selected region where there are nanocapsules on the PCL nanofiber surface, as illustrated in Figure 3.5. The EDX spectrum shows the presence of carbon (PCL polymer) and silver, due to the presence of nanoparticles. Aluminum, silicon and platinum are the chemical elements of the substrate.

Therefore, a nanosystem composed of PCL nanofibers containing AgNps embedded in the bulk and functionalized on their surface with the AgNps-Nanocapsules was successfully achieved.

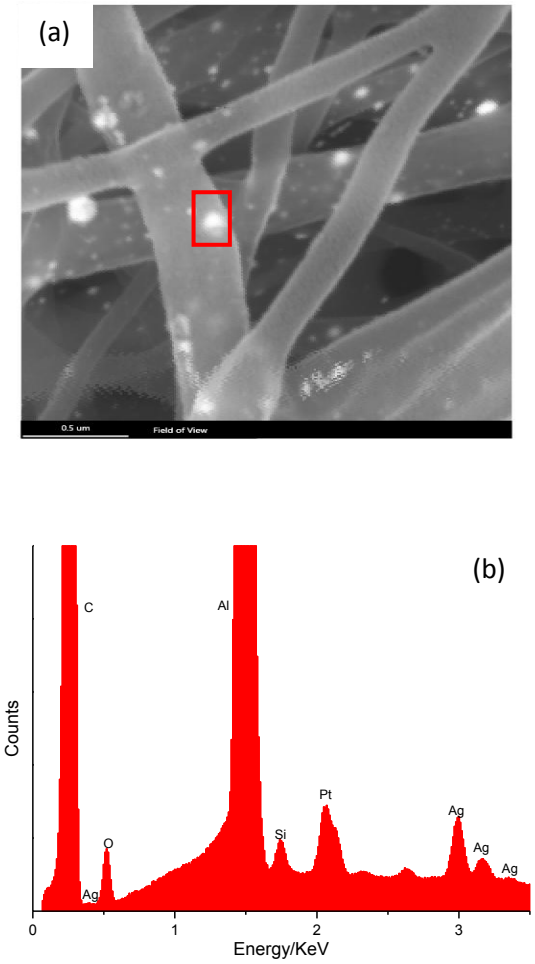

Figure 3.5 - EDX spectra of AgNps-Nanocapsules functionalized on the nanofiber surface. It is determined the chemical composition of the nanosystem.

Source: By the author.

The schematic diagram in Figure 3.6 illustrates the mechanism of silver nanoparticles release by photoactivation during the laser irradiation. The AgNps are released and diffused

through the nanofiber mats to the environment or host, avoiding the bacterial growth around the nanofibers mats, figure 3.6.

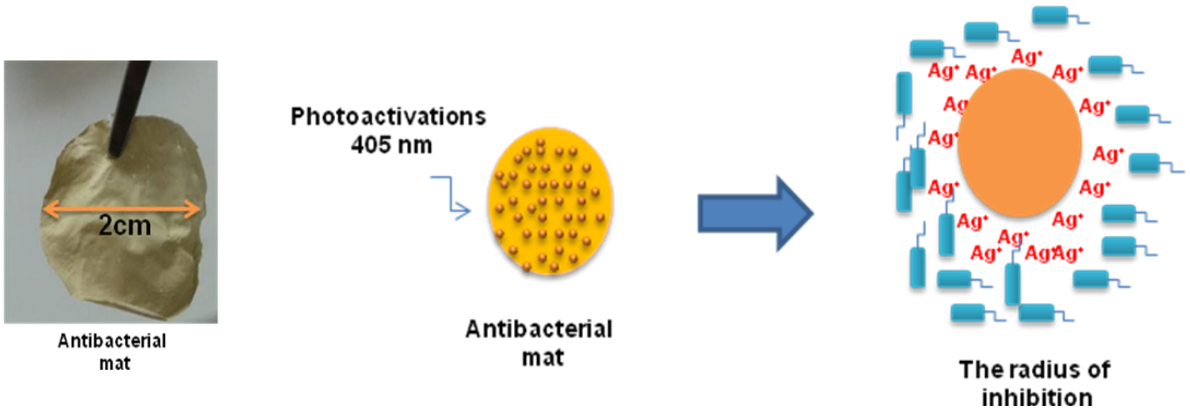

Figure 3.6 - Schematic diagram of release of silver nanoparticles from the nanofibers induced by photoactivation.

Source: By the author.

The 405 nm laser source was applied on nanofibers/AgNps-nanocapsule mat during 150 s to release the AgNps (figure 3.7a). Nanofibers mats before and after irradiation were displayed in FESEM images, figure 3.7b and c. The smooth surface (without nanocapsules) of nanofibers in Figure 3.7c indicates that the majority of AgNps were released when light was applied. Consequently, the AgNps were diffused through the nanofibers. Such result is interesting for antibacterial applications, once it makes possible the control of silver ions release from the nanosystem using specific excitation wavelength, density power, doses and time. This method avoids the direct interaction of AgNps with cells and tissues, decreasing possible toxic effects of AgNPs. In addition, the biodegradable and biocompatible properties of PCL nanofibers allow to use this system without generating toxic effects for biomedical applications.[118]

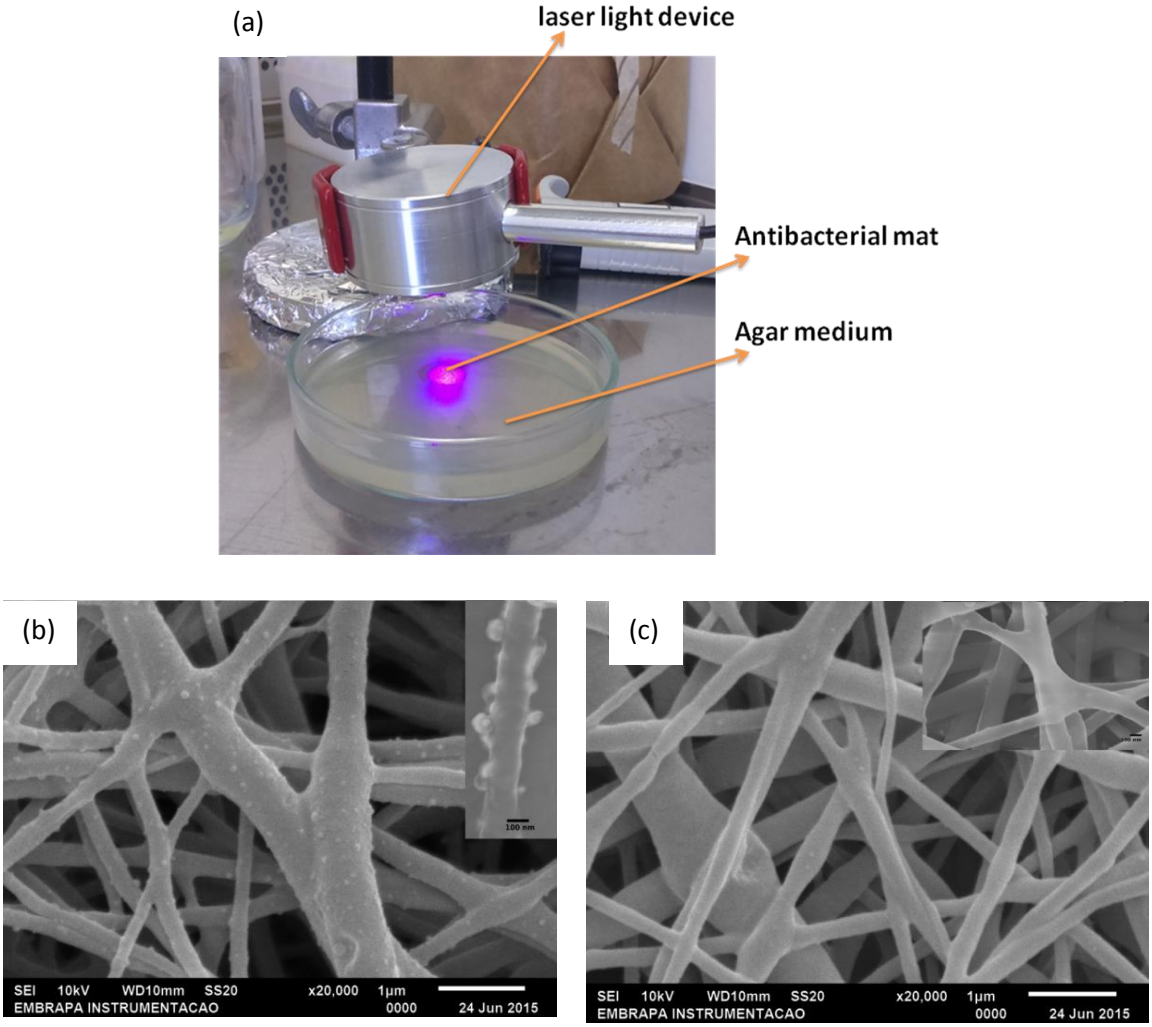

Figure 3.7 - FESEM images, (a) laser irradiation over antibacterial mats, PCL nanofibers functionalized with AgNps-nanocapsules (b) before and (c) after laser irradiation (405 nm) during 150 s to room temperature.

Source: By the author.

3.5.3 Antibacterial Applications

The antibacterial properties of the AgNps-Nanocapsules and PCL nanofibers were investigated by Agar diffusion test through the evaluation of the inhibition zone around the disk after incubation at 37 ˚C. Eight groups were considered to study the bacterial inhibition: (1) Control sample, (2) laser irradiation, (3) Nanofibers without AgNps-nanocapsules, (4)

Nanofibers with nanocapsules without irradiation, (5) Nanofibers with nanocapsules and irradiation, (6) nanofiber/nanocapsule, (7) AgNps-PCL nananofiber and (8) irradiated PCL nanofiber/nanocapsule, as displayed in table 3.1 and figure 3.8.

Table 3.1 - Eight groups were considered to study the bacterial inhibition.

Groups	Name of sample	Description
1	Control sample	*E. coli* and *S. aureus* bacteria
2	Laser irradiation	Laser irradiation over control sample
3	Nanofibers without AgNps-nanocapsules	PCL Nanofibers without AgNps and AgNps-nanocapsules
4	Nanofibers with nanocapsules without irradiation	PCL nanofiber functionalized with AgNps and AgNps-nanocapsules without irradiation
5	Nanofibers with nanocapsules and irradiation	PCL nanofiber functionalized with AgNps and AgNps-nanocapsules with irradiation
6	nanofiber/nanocapsule	PCL nanofiber functionalized with nanocapsules (without AgNps) with irradiation
7	AgNps-PCL nananofiber	PCL nanofiber functionalized with AgNps
8	PCL nanofiber/nanocapsule exposed to irradiation	PCL nanofiber functionalized with AgNps-nanocapsules with irradiation

Source: By the author.

Groups 4, 5, 7 and 8 showed bacterial inhibition, which is due to the AgNps, nanocapsules and the Ag ions on the nanofibers. Sample 5 showed antibacterial activity against *E. coli* and *S. aureus*, with an inhibition radius of 1.78 ± 0.49 mm and 2.58 ± 0.28 mm, respectively, as illustrated in figures 3.9 and 3.10.

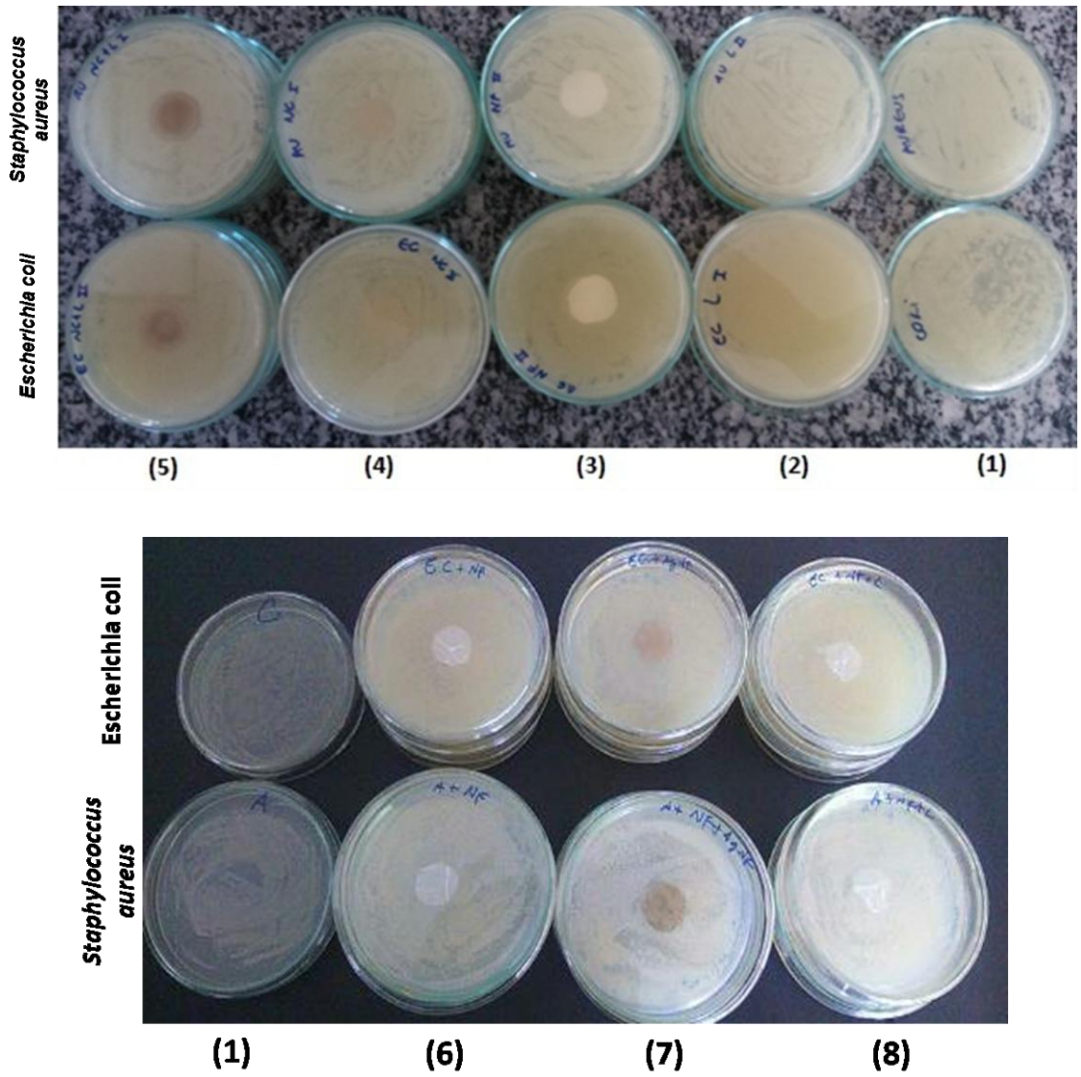

Figure 3.8 - Eight groups of samples investigated regarding bacterial inhibition; (1) Control, (2) LASER irradiation, (3) Nanofibers without AgNps-nanocapsules, (4) Nanofibers with nanocapsules without irradiation, (5) Nanofibers with nanocapsules and irradiation, (6) PCL nanofiber/nanocapsule, (7) AgNps-PCL nananofiber and (8) PCL nanofiber/nanocapsule with irradiation.

Source: By the author.

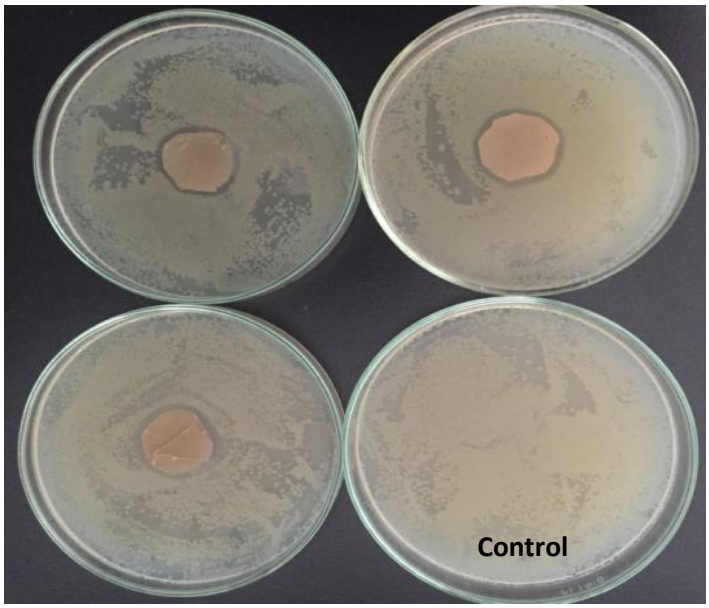

Figure 3.9 - Bacterial inhibition in Gram-negative *Escherichia Coli* of nanofibers/AgNps-nanocapsules after exposition to laser excitation at 405 nm. The radius of inhibition region was 1.78 ± 0.49 mm.

Source: By the author.

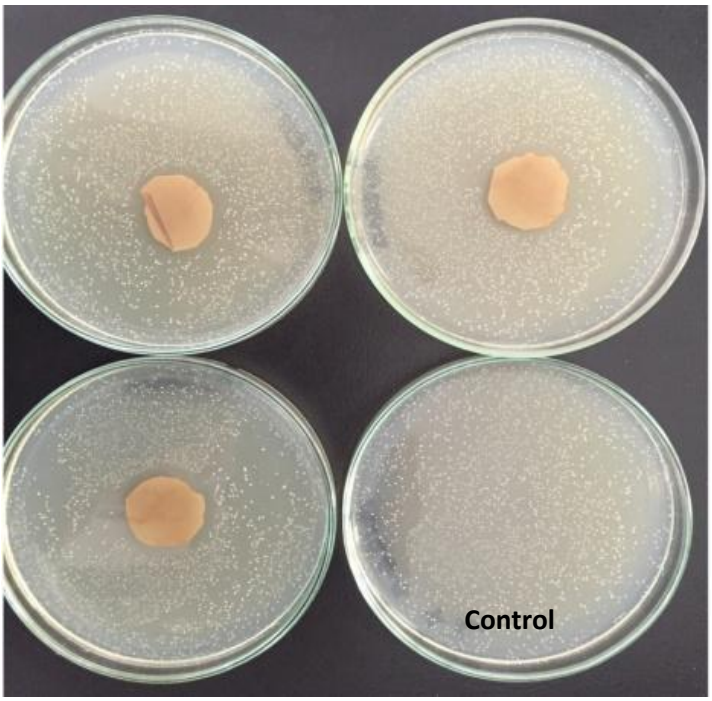

Figure 3.10 - Bacterial inhibition in *Gram-positive Staphylococcus Aureus* of nanofibers/AgNps-nanocapsules after exposition to laser excitation at 405 nm. The radius of inhibition region was 2.58 ± 0.28 mm.

Source: By the author.

AgNps can easily diffuse on nanofibers mats and act as biocidal agents.[119] The nanoparticles release silver ions with antibacterial properties via mechanisms such as interaction with cell membrane or binding with metabolic materials, preferentially on thiol groups, causing destruction of the membrane and increasing permeability and cytoplasm leak.[120]

Recent papers show antibacterial mats composed of silver nanoparticles with inhibition radius greater than ours,[121 - 123] this is due to a high concentration and exposure of the nanoparticles to the bacterial medium.[124 - 126] Despite our system does not have a high concentration of nanoparticles, it has the ability to release AgNps in a controlled manner after irradiation, these nanoparticles are dispersed in the nanofiber mat generating an inhibition radius considered optimal for biomedical application such as wound healing.[127 - 130]

3.6 Conclusion

The smart antibacterial nanosystem developed can be stimulated by laser excitation at 405 nm to release AgNPs. The excitation of the SPR (AgNps) produce electronic vibrations that break the cross-linking between the Aniline and the Chitosan molecules of the nanocapsule, leading to AgNps release on the nanofiber surface. The control in the AgNps release allows the constructions of multifunctional nanoplatforms, employing the photosensitive properties of the AgNps-Nanocapsules immobilized on the PCL nanofiber.

As an application of the antibacterial properties of the PCL nanofiber mats, tests were carried out against the inhibition of Gram-negative and Gram-positive bacteria using Agar diffusion test. The nanofiber mats present bacterial inhibition for samples 4, 5,7 and 8. On the other hand, sample 5 (nanofibers with nanocapsules and irradiation) presented bacterial activity against *E. coli* and *S. aureus,* indicating its potential for biomedical applications. This result suggests a potential use of the nanofibers/nanocapsules and irradiation in therapy avoiding the toxic effects of the direct interaction of AgNps with human skin on infections after surgeries and wounds.

4 Interaction of nanocapsules with cell membrane models

4.1 Langmuir films

Langmuir films are monolayers of an amphiphilic material, *i.e.* a molecule with a polar head (hydrophilic) and an apolar tail (hydrophobic), organized at a liquid-liquid or gas-liquid interface. Usually the liquid phase (subphase) is composed by water. Examples of amphiphilic molecules are the soaps and phospholipids.[131] The formation of Langmuir films usually requires an equivalent proportion between the polar and apolar parts of the molecules, or equivalent in charged chemical groups,[132] to establish the monolayer. Another important parameter is the deposition of a fixed volume of the solution in a volatile and immiscible solvent, dispersed on a subphase in an inert device (Langmuir trough). For example, in the subphase with water, it can be used chloroform as solvent.[132]

The Langmuir trough is usually made of Teflon with mobile barriers, where the position and velocity of compression can be computer-controlled. Pressure and surface potential can be monitored, as displayed in figure 4.1. The surface pressure (Π) is defined as the difference of surface tension between the subphase with pure water (γ_0) and the subphase with the film (γ), $\Pi = \gamma_0 - \gamma$.[132] This pressure can be obtained by measuring the force per unit of length on the fixed barrier using an electrobalance, or measuring the surface tension by Wilhelmy method.[132] The minimum surface pressure measured is 0 and maximum can be close to the surface tension in pure water (25 ^{o}C), approximately of 73 mN/m.[133]

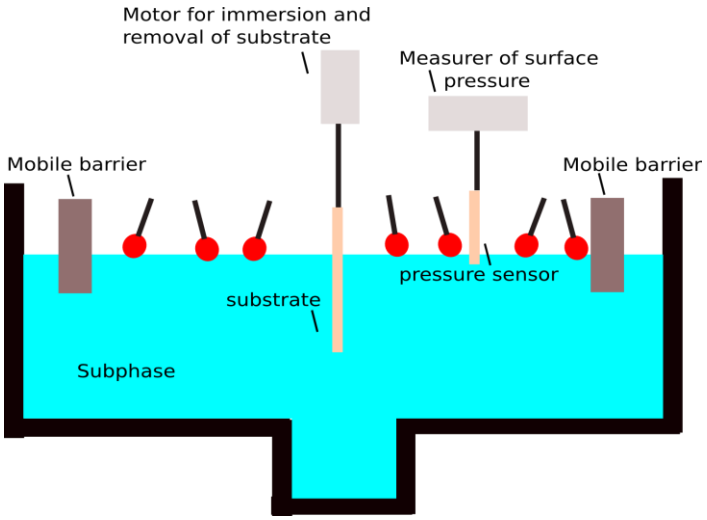

Figure 4.1 – General scheme of Langmuir through.

Source: By the author.

The compression of the film, through the movement of the mobile barriers, can orientate the molecules perpendicular to the water surface. A film without compression has a behavior similar to a two-dimentional gas, since the molecules are dispersing on the surface and there are no interactions between them.[132] This initial stage is called gas phase, and with a initial compression (decreasing the area occupied by the monolayer), the expanded-liquid phase[132] can be reached. By increasing the compression of the barriers, the molecules start a regular arrangement of the condensed film (condensed-liquid film). However, after a certain point, the breakdown of the monolayer, known as collapse, can occur.[132] Consequently, the phases of the film can be related to the regions of the surface pressure isotherm, *i.e.* the pressure (Π) versus the area per molecule of the film ($Å^2$/molecule), as illustrated in figure 4.2

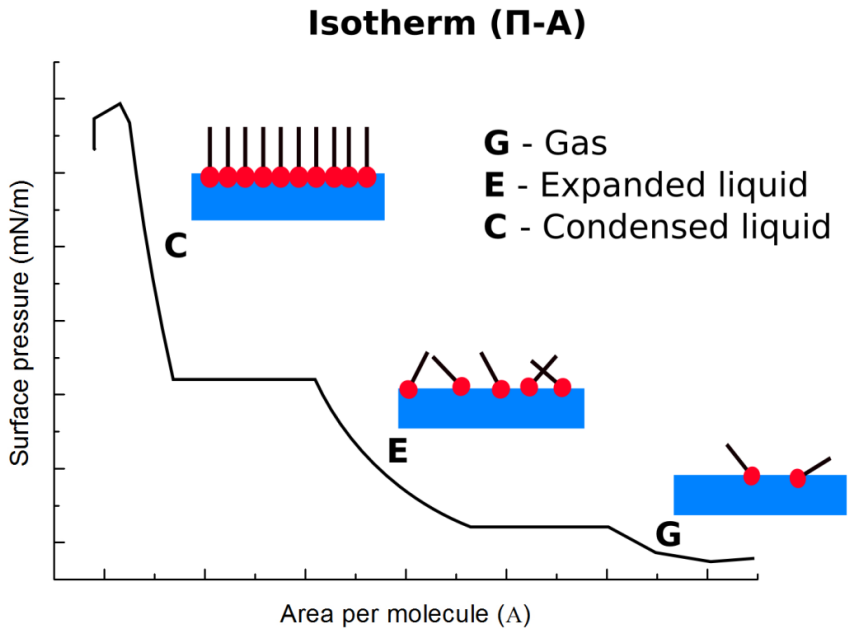

Figure 4.2 – Ideal isotherm model.

Source: By the author.

The velocity employed during the compression of the barriers in the Langmuir trough, as well as the time of compression are fundamental for the arrangement of molecules on the surface, producing a packaging close to the thermodynamic equilibrium.[132] The hysteresis curve are a repetitive process of the cycles of compression and decompression of the molecules (the barriers of the Langmuir trough are closed and opened repeatedly) on the water surface.[132] The stability studies of the films are performed by the observation of the area per molecules of the compressed film to a given surface pressure, usually in the expanded-liquid phase as a function of time.[132] In stable films, the variations in area are minimal as a function of time.[28]

Langmuir technique has been widely applied to understand the behavior of nanomaterials upon interaction with cell membrane models.[134 - 135] The mechanism of action of the nanomaterials can be determined and designed from its specific interaction (or not) on

membrane models.[136] This knowledge is relevant to further understand the mechanisms related to cell uptake for antibacterial and biomedical purposes.[136 - 138]

4.2 Experimental

4.2.1 Kinetics of AgNPs release using a LED source at 405 nm

The kinetics of release of AgNps was studied using a diode LED (LHUV-0405) at 405 nm with an intensity of 32 mW/cm^2. The diode LED is placed 5 cm distant from the nanocapsules dispersion (0.9 µg/mL). For the measurements, 500 µL of nanocapsules dispersion (0.9 µg/mL) contained in a glass cuvette were irradiated at intervals of 30 s, during 600 s, changing the dispersion sample for every measurement, for which the samples were monitored by UV-Vis absorption spectroscopy (405 nm) at room temperature. The time for complete release was estimated at 240 s.

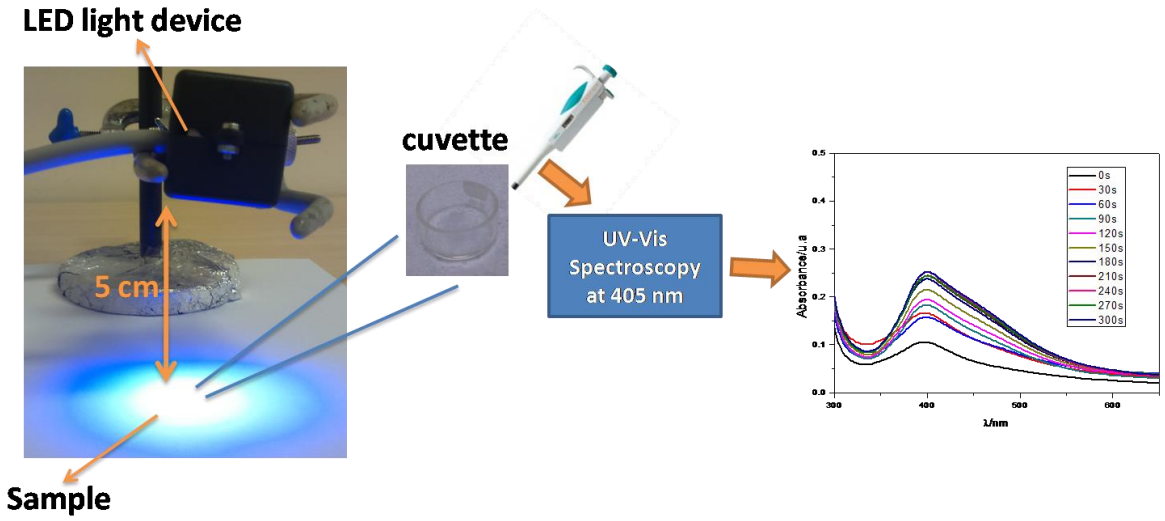

Figure 4.3 - Schematic representation of LED source at 405 nm used to study the release of Ag nanoparticles and data collection.

Source: By the author.

4.2.2 Kinetics of AgNPs release using excitation at 405 nm on the Langmuir trough

For the evaluation of the kinetics of AgNps release on the Langmuir trough a tool of aluminum box with diode led was set over the trough for irradiation of the subphase, as displayed in figure 4.4(a) and (b). The diode led is maintained at a distance of 5 cm and applied light during 240 s as is explained before.

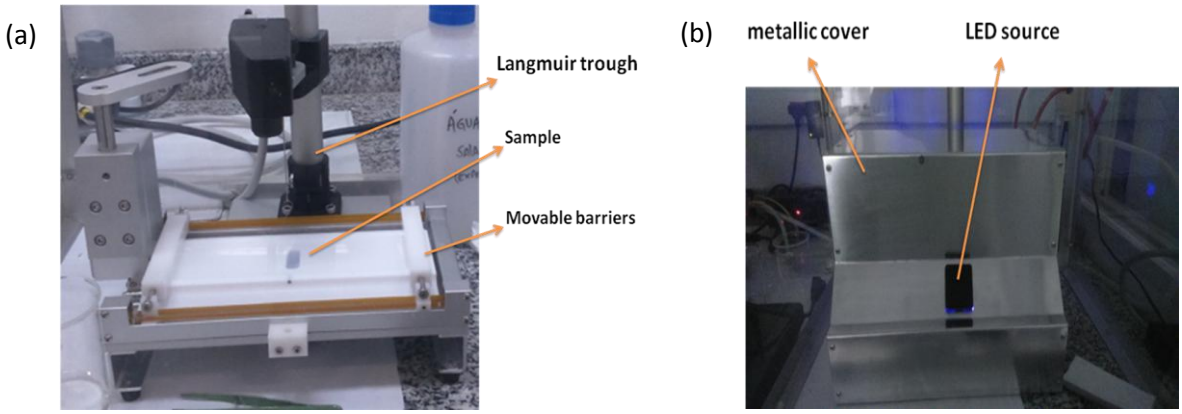

Figure 4.4 – Illustrations of Langmuir trough and LED for membrane model experiments. (a) open (b) closed with a metallic cover.

Source: By the author.

4.2.3 Minimum inhibitory concentration (MIC) for *Escherichia coli*

For minimum inhibitory concentration (MIC) experiments, the AgNps-nanocapsules were dissolved in 100µl of Mueller Hinton Broth to obtain a concentration of 57.6 µg/ml in the first well. Next, a two-fold dilutions series were carried out using a microtiter plate until the 8^{th} well reached a concentration of 0.45 µg/mL. 10µl of the microorganism was added to a final concentration of $1\text{-}5\times10^{4}$ cells/ml on each well.

In our experiments, the effect of light irradiation on the microtiter plate was investigated, once the release of AgNps is expected to occur, enhancing the antibacterial effect, figure 4.5. Therefore, tests are carried out using a plate with and without irradiation.

The growth of bacteria was hourly monitored by UV-Vis absorption spectroscopy (at 625 nm) during 12 h. This experiment is compared with the membrane models experiment to determine the effect of the nanocapsules on the antibacterial mechanism (with and without light irradiation).

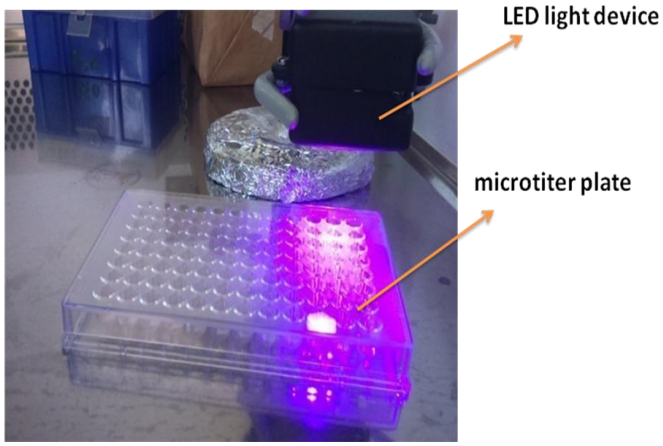

Figure 4.5 – Led irradiation over microtiter plate used in the investigation of release of AgNps for antibacterial studies.

Source: By the author.

4.2.4 Membrane models

To develop the experiments, two phospholipids were chosen with different charges. 1,2-dimyristoyl-sn-glycero-3-phosphoethanolamine (DMPE) with zwitterinc characteristics, which has positive and negative charges[139] and 1,2-dipalmitoyl-sn-glycero-3-phospho-(1'-rac-glycerol) (DPPG) with anionic characteristic,[140] whose chemical structures are displayed in figure 4.6. Both were used in the concentration of 1 µmol/L, while DMPE was solubilized in chloroform and DPPG in methanol: chloroform in the proportion of 1:4 (v/v). The variation of surface pressure was recorded as a function of the available area per molecule, for the construction of the surface isotherm.

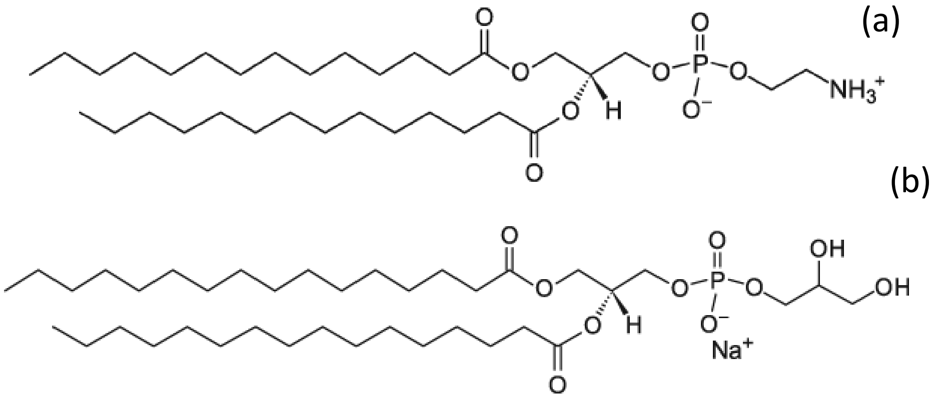

Figure 4.6 – Molecular representation of DMPE (a) and DPPG (b).

Source: AVANTI…[141]

The experiments were performed at 21 ± 1 ℃. The isotherms of area-surface pressure (Π-A) was obtained by dispersing 6 µL of the phospholipids in the water surface using a Hamilton microsyringe. After 5 min of the evaporation of the organic solvent, the barriers were compressed and decompressed using a velocity of 10 mm/min until a surface pressure of 50 mN/m or 0 mN/m was reached by 3 cycles. For the analysis of the interaction of nanomaterials, the unique change was the addition of the nanomaterials on the subphase and application of LED at 405 nm when necessary.

4.3 Results and discussion

4.3.1 Kinetic of release of AgNps

To investigate the interaction of AgNps with the membrane models, it was necessary to determine the time of release of AgNps from the nanocapsule by applying light of LED at 405 nm. In this case, the LED source was preferably employed due its better ability to scatter light and shine the sample, instead of using a laser source. The kinetics of release of AgNps was determined by UV-Vis absorption spectroscopy, monitoring the absorption at 405 nm, which represents the SPR of the AgNps. The LED light was applied at every 30 s until 600 s on a dispersion of AgNps-Nanocapsule in a concentration of 0.9 µg/mL. After excitation, an

increase of intensity in the plasmon band of the AgNps can be observed by UV-Vis spectra, as illustrated in figure 4.7a. This increase in intensity can be generated by the detachment of AgNps, due to the electronic vibration of the LSPR produced from inside the nanocapsule as mentioned in section 3.3.1. The time of release of Ag nanoparticles was determined at 240 s, which represent a totally detachment of the nanoparticles from the nanocapsule, Figure 4.7b.

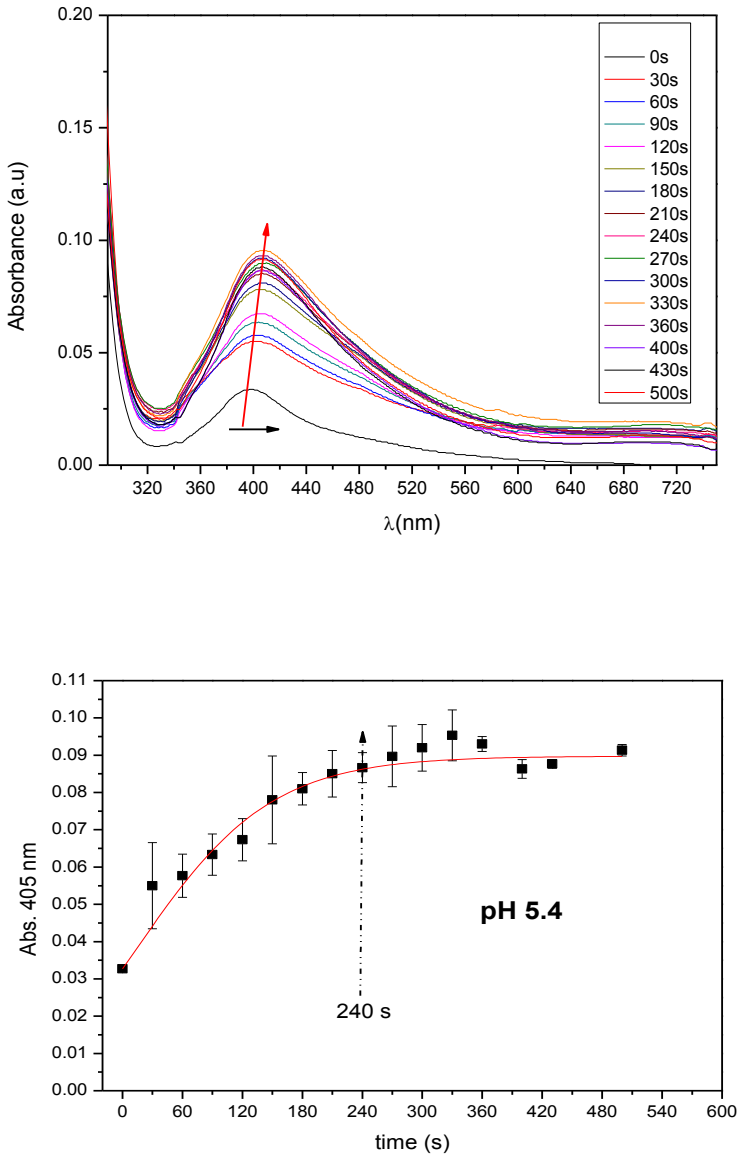

Figure 4.7 - Photoactivation of AgNps-Nanocapsules, (a) UV-Vis spectra of the kinetics of release of AgNps (b) the kinetic of release shows a stabilization at 240 s where most of the nanoparticles are released.

Source: By the author.

4.3.2 Minimum inhibitory concentration

To determine the minimum inhibitory concentration of AgNps-Nanocapsules, the experiments with and without LED excitation over *E. coli* were carried out as described in section 4.2.3. The curve of bacterial concentration as a function of nanoparticles concentration is displayed in figure 4.8. It is observed that irradiated samples present a lower concentration of bacteria compared to non-irradiated samples, once in the first case AgNps are released in the medium, increasing the bacterial death. The minimum inhibition concentration[142] for the two experiments was determined as 0.9 µg/mL. According with Wen-ru Li et al,[143] a concentration of 10 µg/mL could completely inhibit the growth of *E. coli*, since AgNps produce the leakage of sugars and proteins and induced the respiratory chain dehydrogenases into inactive state, suggesting that AgNps were able to destroy the permeability of the bacterial membrane.[143, 60 - 61] Therefore, this concentration (0.9 µg/mL) will be used in membrane model experiments as a way to mimic the concentration that damages the membrane of *E. coli*.

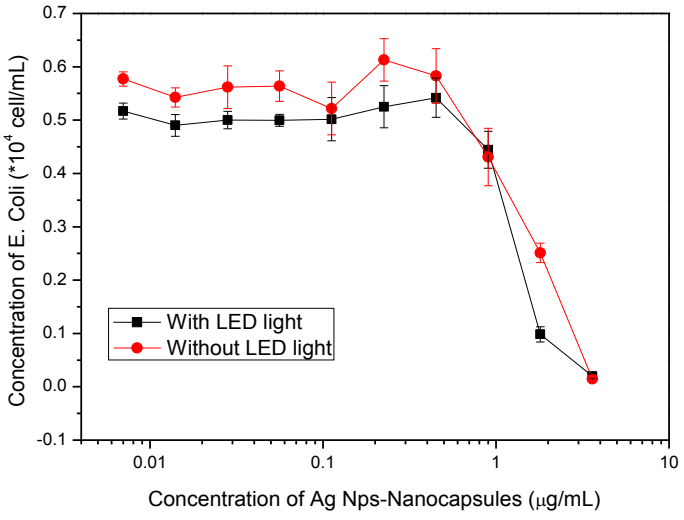

Figure 4.8 – Curve of bacteria growth as a function of AgNPs nanocapsules concentration for samples with and without exposition to LED excitation at 405 nm. MIC was determined as 0.9 µg/mL.

Source: By the author.

4.3.3 Membrane models

Many studies have been carried out to analyze the cell membrane properties using models like liposomes or lipid molecules.[144] The studies on lipid monolayers can be carried out using the Langmuir technique, allowing the fabrication and characterization of films of amphiphilic molecules with control in packing density. Several information can be obtained by isotherms measurements including molecular area, structural changes, phase transitions, compressibility and hysteresis.[136]

Langmuir films have advantages over others membrane models as the study of molecular interaction in the surface of the membrane models, allowing the understanding of kinetics interaction at the bio-nano interface in realtime.[132] There are experimental observations and theoretical studies of the similarity of monolayers with the arrangement of the membrane, whereby the Langmuir films occupied the same area with alignment and compaction that molecules do in the membrane cell.[132] However, Langmuir monolayers have some disadvantages because this model only permits the simulation of the half of the cell membrane, which is deficient to studies of molecular transport through the membrane.[30, 145]

The lipidic dependence in the interaction with nanomaterials is a very important question because it allows to evaluate the entry or not of these materials inside the cells. The DMPE and DPPG lipids were used to study the interaction with the AgNps-nanocapsules shown in chapter 2. This nanosystem has a differentiated behavior when it is irradiated at 405 nm. In this case, the surface plasmon band of AgNps is excited by the irradiation, detaching this nanomaterial of the polymeric matrix or nanocapsule. By knowing this behavior, the interaction at the molecular level mimicking a membrane of *E. coli* bacteria is possible, once it is composed basically of 58% of DMPE lipids, 16% of DPPG lipids, 9% of cardiolipin lipids and 18% of others lipids.[141] Firstly, it is evaluated the interaction of AgNps-Nanocapsules with DMPE and DPPG lipids individually, following the evaluation of the binary mixture using the same proportion of the bacteria in order to observe the lipid influence in this interaction.[146] The concentration of AgNps-Nanocapsules used in this study was those determined by MIC for *E.Coli*.

Figure 4.9 shows the kinetics of the interaction between DPPG and AgNps-Nanocapsules (NC) with and without using the LED source (a), the isotherm of the systems (b) and the compression and decompression (c). The isotherms were obtained for a DPPG monolayer on

aqueous subphase in the absence and presence of nanomaterials. The barrier velocity was maintained at 10 mm/min and the monolayer was subjected to 2 successive cycles of compression and decompression.

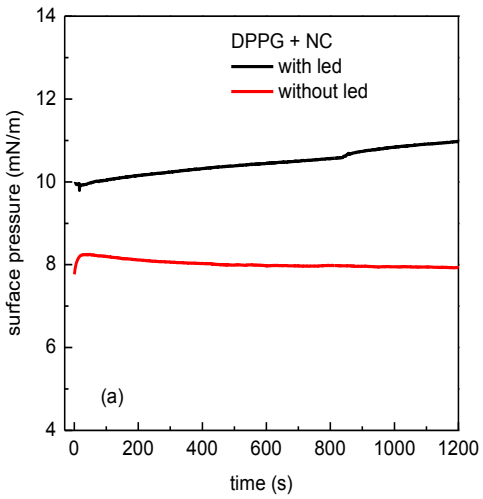

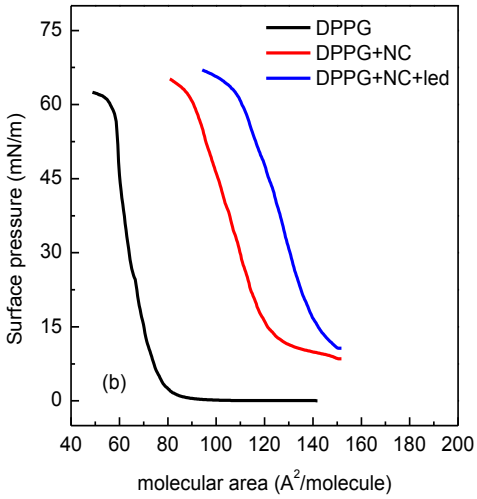

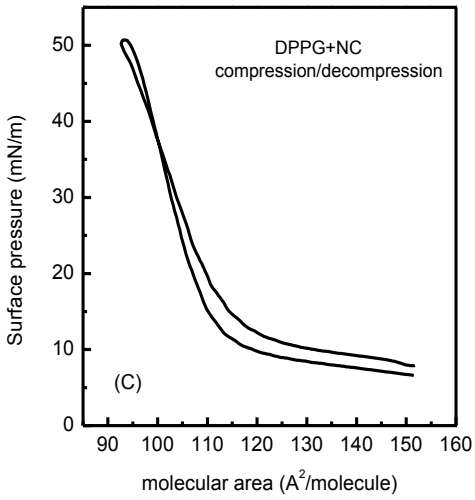

continue

continuation

(d)

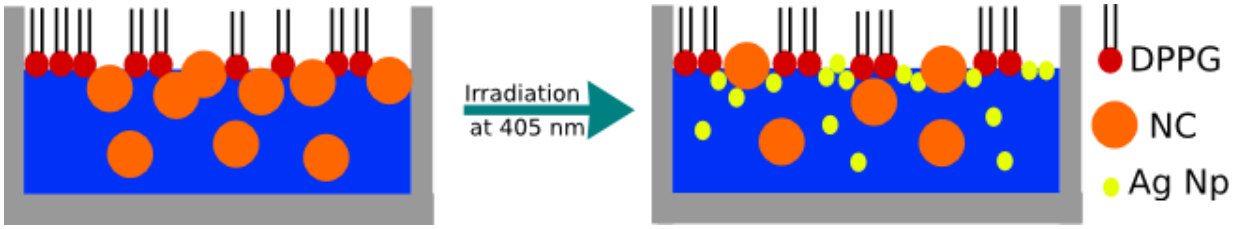

Figure 4.9 - (a) kinetics, (b) isotherm and (c) compression and decompression of the interaction of DPPG monolayer with AgNps-Nanocapsules (NC). (d) schematic diagram of the behavior of AgNps with DPPG before and after irradiation.

Source: By the author.

Figure 4.9a shows the surface pressure vs the time variation of the DPPG monolayer with AgNps-Nanocapsules, applying or not the LED excitation for 240 seconds. It is possible to verify a significant variation in the surface pressure vs time when the LED excitation is applied, where the surface pressure increase from 8 mN/m to 11 mN/m. This fact may be related to the detachment of the AgNps from the polymeric network, increasing the surface tension. Large variation in the molecular area is observed in the isotherms in figure 4.9b. For a certain surface pressure there is a variation in molecular area; for example, when the DPPG monolayer is compressed in a surface pressure of Π = 30mN/m, there is a molecular area of 65 $Å^2$/molecule. In contrast, when there is AgNps-Nanocapsule in the subphase, an increases in the molecular area of 110 $Å^2$/molecule is observed, and this value increases even more when the LED is applied (130 $Å^2$/molecule) for the same surface pressure. This behavior suggests that the monolayer composed of DPPG lipids is extremely affected by the presence of the AgNps release in the subphase, and apparently there is an incorporation of the AgNps between the lipids (figure 4.9d), causing that the monolayer to be less packed compared to the monolayer without the AgNps-Nanocapsules. However, the movement of the barriers did not impair the interaction during compression and decompression of the monolayer, as observed in figure 4.9c.

On the other hand, the monolayer constituted by DMPE did not present significant differences in the surface pressure variation or in the molecular area of the isotherms. The

figure 4.10 shows the kinetics and the isotherms of the interaction between the DMPE lipid with the AgNps-Nanocapsules.

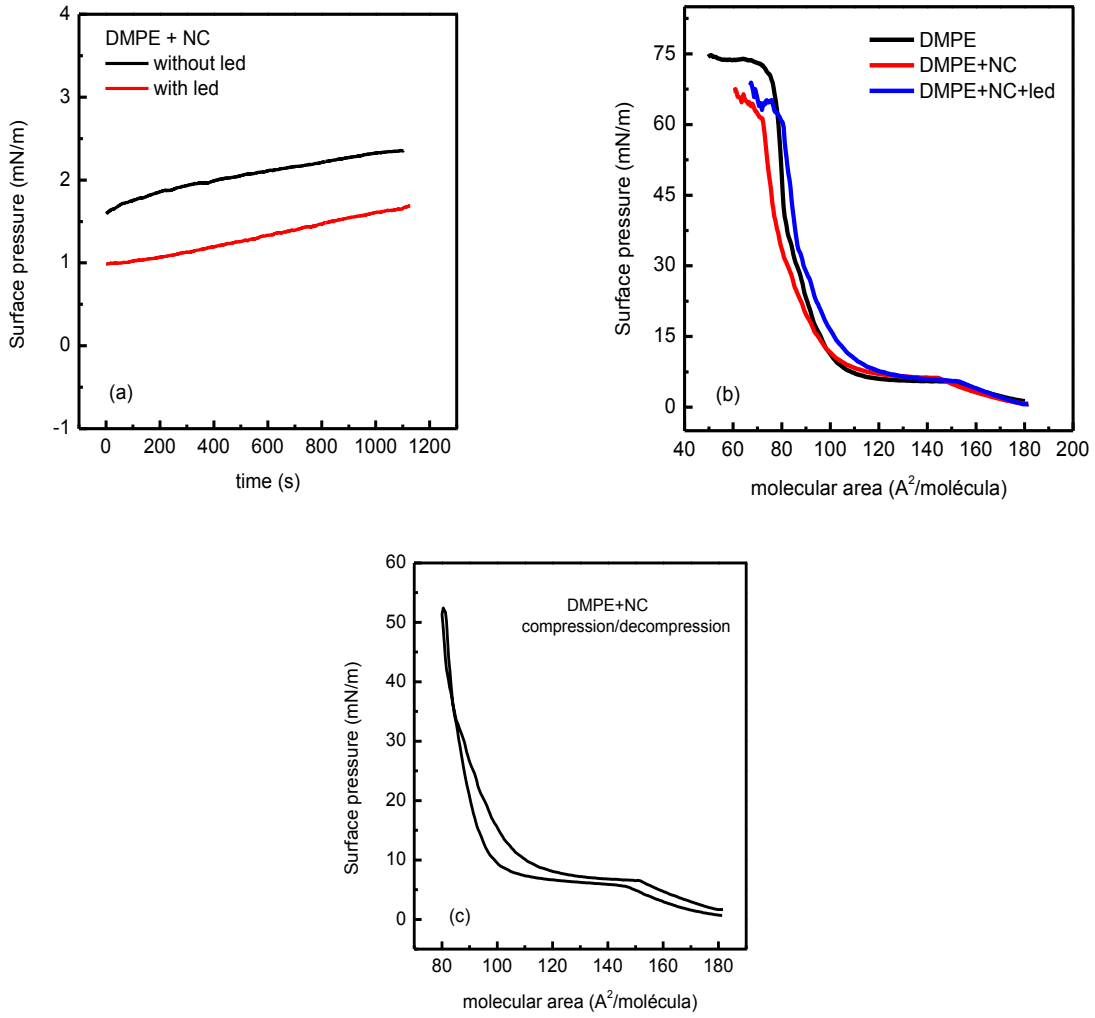

continue

continuation

(d)

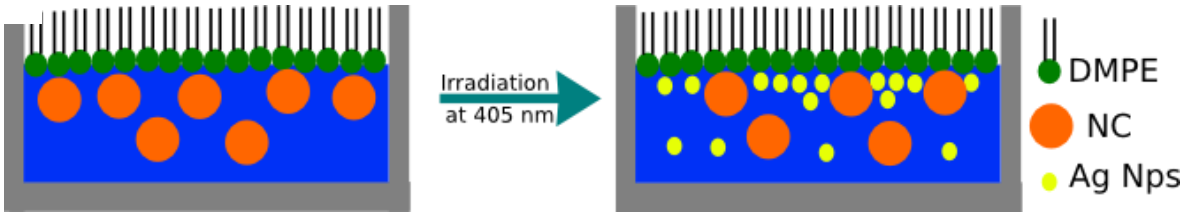

Figure 4.10 - (a) kinetics, (b) isotherm and (c) compression and decompression of the interaction of DMPE monolayer with AgNps-Nanocapsules. (d) schematic diagram of the behavior of AgNps with DMPE before and after irradiation.

Source: By the author

.

Values of surface pressure of the kinetic profile of the interaction between DMPE and AgNps-Nanocapsules also increase with the time; however this variation was smaller than with the DPPG system. The isotherms of figure 4.10b show that the DMPE monolayer lipid packaging was not changed, even after the application of the LED light. In this case, a small variation in the molecular area of nearly 8 $Å^2$/molecule was observed for the surface pressure of 30 mN/m. This behavior may be associated with the repulsive electrostatic effects between AgNps-Nanocapsules (amine groups) and lipid molecules that have positive charges (figure 4.10d), leading to an unstable behavior during compression and decompression. A decrease in the molecular area values in the decompression of the monolayer occurs as a function of the surface pressure, as shown in figure 4.10c.

After analyzing the interaction between AgNps-Nanocapsules and the DPPG and DMPE lipids individually, we investigated the effects of the nanomaterials in a mimicked monolayer of *E. Coli*, which is composed of different proportion between the lipids DPPG (16%) and DMPE (58%). The results are shown in figure 4.11.

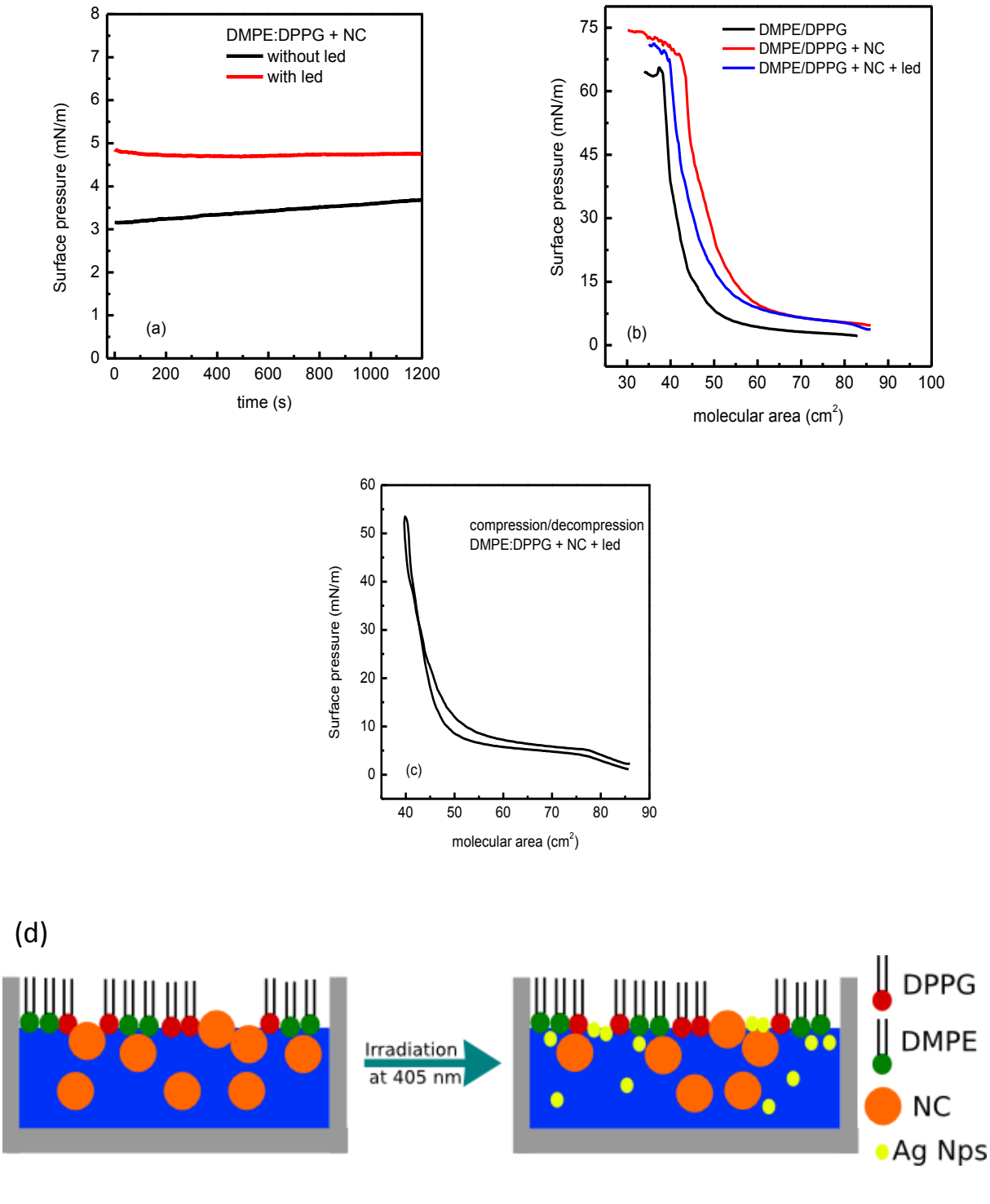

Figure 4.11 - (a) kinetics, (b) isotherm and (c) compression and decompression of the interaction of DMPE:DPPG monolayer with AgNps-Nanocapsules. (d) schematic diagram of the behavior of AgNps with DPPG:DMPE before and after irradiation.

Source: By the author.

Figure 4.11a shows the surface pressure vs time of the binary monolayer composed of the lipids DPPG:DMPE and AgNps-Nanocapsules, with and without exposition to LED light. It is possible to verify a variation of at least 2 mN/m in the surface pressure when the LED excitation is applied, which is a similar variation to the observed for the DPPG system (figure 4.9). In the isotherms, is observed a variation in the area of at least 10cm^2 for a surface pressure of 30mN/m. In contrast, when LED excitation is applied, for the same surface pressure, a small variation in the area of 5 cm^2 is observed, figure 4.11b. This behavior was expected, because there is the contribution of the two lipids in the interface. The pressure and surface tension behavior is highly influenced by the physico-chemical characteristics of the lipid molecules. Since there are two lipids in the monolayer, the organization of these molecules in the subphase are affected by variations in the size, interaction between nanoparticles and the molecules. In fact, the contribution of the DPPG molecules in this interaction is very strong, mainly due to the electrostatic interaction between the charges of the lipids and the AgNps, figure 4.11d. The nanomaterials are located between the phospholipids (DPPG), breaking the structure of the membrane model.

4.5 Conclusions

In this chapter we reported the interaction of nanocapsules with cell membrane models. Specifically, we have determined the time of release AgNps from the nanocapsule by applying light of a diode led at 405 nm. The release of AgNps was monitored by UV-Vis absorption spectroscopy. After irradiation, an increase of intensity in the plasmon band of the AgNps was observed, which is caused by the detachment of AgNps from the nanocapsule. The time of release was determined at 240 s, which is important for studies in model membrane. The consequences of the irradiation to the AgNps-Nanocapsules in the presence of *E. coli* was also investigated. Upon irradiation of the nanocapsules, a release of AgNps was observed, increases the death of bacterial. The minimum inhibition concentration was determined at 0.9 µg/mL for the two experiments (with and without light).

The studies of membrane models showed different behavior for each type of lipid (DPPG, DMPE and DPPG:DMPE) when interacting with the AgNps-Nanocapsule exposed on not to LED excitation. It is observed that the monolayer composed by DPPG lipids was affected by the presence of the AgNps-Nanocapsule in the subphase, indicating the

incorporation of the Ag nanoparticles between the lipids. Also, under irradiation, a less packed configuration was found compared to the monolayer without the nanocapsule. On the other hand, the monolayer constituted by DMPE did not present significant differences in the surface pressure variation. This effect can be associated with the repulsive electrostatic effect between the nanocapsules and the lipid molecules that have positive charges. The binary monolayer composed of DPPG:DMPE showed similar behaviors with the DPPG monolayer, which allows an electrostatic interaction between these molecules and the Ag nanoparticles. These results suggest that DPPG has more influence on the incorporation of the nanoparticles on the cell membrane.

5 Conclusions and Perspectives

In this thesis, we have demonstrated the fabrication of Ag-Nps Nanocapsule and nanofibers embedded with AgNPs for developing a smart nanosystem aiming at antibacterial application. Specifically, the research was focused in the development of nanomaterials with antibacterial properties with high control of the size, shape and morphology, aiming to tune the release time of nanomaterials when interacting with light at 405 nm and also to investigate the mechanism of action on cell death.

First, two types of nanomaterials are synthesized: the AgNps-nanocapsule and polycaprolactone nanofibers containing AgNPs. The AgNps-Nanocapsule were synthesized by the cross-linking between aniline and chitosan in a hybrid polymeric nanocapsule loaded with silver nanoparticles. The cross-linking attachment between protonated amine groups of aniline and chitosan and OH^- of chitosan was achieved, producing a nanogel structure. This smart nanomaterial has a SPR that can be stimulated by light at 405 nm. On the other hand, PCL nanofibers embedded with AgNps were fabricated with good homogeneity and stability. The nanofibers morphology is optimal for antibacterial application, once they have a similar structure of proteins expressed by bacteria that form the biofilm. With the assembly of these two nanomaterials, it was possible to create a smart nanomaterial that can be used as an antibacterial system activated by light irradiation.

Secondly, we studied the release of AgNps when the AgNps-nanocapsules were irradiated with a light at 405nm using a diode laser. The localized surface plasmon of the nanoparticles was driven into resonance, producing an increase of kinetic energy of the nanocapsule. This effect breaks the nanocapsules and as a consequence releases the nanoparticles. A later stage, the AgNps-Nanocapsules were immobilized on the PCL nanofiber surface and irradiated at 405nm, which also produced the release of AgNps inside of the nanofiber mats. These antibacterial nanofiber mats were tested against *Gram-negative Escherichia coli* and *Gram-positiva Staphylococcus aureus*, indicating its antibacterial properties.

Finally, the kinetics of release of AgNps from nanocapsules irradiated by a 405 nm LED was also investigated. The minimum inhibitory concentration (MIC) of the AgNps-nanocapsule dispersion was determined for Gram-negative *Escherichia Coli*. On the other hand, the behavior of these nanomaterials was investigated using membrane models combined to the Langmuir technique. It is observed that the monolayer composed by DPPG lipids was affected by the presence of the AgNps-Nanocapsule in the subphase, caused by the incorporation of the Ag nanoparticles between the lipids. Therefore, the perturbation in the membrane model can be associated to the incorporation of nanoparticles between DPPG molecules.

Given the interesting antibacterial properties of the smart nanosystem developed, it presents a strong potential for biomedical applications, including wound healing systems. For instance, the antibacterial mats could be placed on wounds and irradiated at 405 nm to release AgNps inside of the nanofiber mat, killing the bacteria and improving the process of cicatrization. In this way, studies in-vivo can be tested to evaluate the healing capacity as well as the possible toxicity.

REFERENCES

1 SORTINO, S. Photoactivated nanomaterials for biomedical release applications. **Journal of Materials Chemistry,** v. 22, n. 2, p. 301-318, 2012.

2 LIN, G. et al. Biodegradable nanocapsules as siRNA carriers for mutant K-Ras gene silencing of human pancreatic carcinoma cells. **Small,** v. 9, n. 16, p. 2757-2763, 2013.

3 CHEN, T.; DU, B.; FAN, Z. Facile fabrication of polymer nanocapsules with cross-linked organic-inorganic hybrid walls. **Langmuir,** v. 28, n. 30, p. 11225-11231, 2012.

4 SHARIFIMEHR, M. R. et al. Preparation and spectral characterization of polymeric nanocapsules containing DR1 organic dye. **Optical Materials,** v. 45, p. 87-90, 2015.doi: 10.1016/j.optmat.2015.02.036.

5 ACHILLEOS, D. S.; HATTON, T. A.; VAMVAKAKI, M. Light-regulated supramolecular engineering of polymeric nanocapsules. **Journal of the American Chemical Society,** v. 134, n. 13, p. 5726-5729, 2012.

6 PELGRIFT, R. Y.; FRIEDMAN, A. J. Nanotechnology as a therapeutic tool to combat microbial resistance. **Advanced Drug Delivery Reviews,** v. 65, n. 13-14, p. 1803-1815, 2013.

7 HAJIPOUR, M. J. et al. Antibacterial properties of nanoparticles. **Trends in Biotechnology,** v. 30, n. 10, p. 499-511, 2012.

8 HUH, A. J.; KWON, Y. J. "Nanoantibiotics": a new paradigm for treating infectious diseases using nanomaterials in the antibiotics resistant era. **Journal of Controlled Release,** v. 156, n. 2, p. 128-145, 2011.

9 MAIA, F. et al. Incorporation of biocides in nanocapsules for protective coatings used in maritime applications. **Chemical Engineering Journal,** v. 270, p. 150-157, 2015.doi: 10.1016/j.cej.2015.01.076.

10 HWANG, S.-W. et al. Biodegradable elastomers and silicon nanomembranes/nanoribbons for stretchable, transient electronics, and biosensors. **Nano Letters,** v. 15, n. 5, p. 2801-2808, 2015.

11 DE BRUM, T. L. et al. Polymeric nanocapsules and lipid-core nanocapsules have diverseskin penetration. **Journal of Nanoscience and Nanotechnology,** v. 15, n. 1, p. 773-780, 2015.

12 POLAAR.University Claude Bernard. Aurelie de Larminat, Daniel Kurbiel, Fabrice Pirot, Elodie Gilbert. **Aqueous suspension of nanocapsules encapsulating sunscreen agents .**US 201601913123,13 Aug. 2014, 07 July. 2016.

13 YUAN, A. et al. Self-assembled PEG-IR-780-C13 micelle as a targeting, safe and highly-effective photothermal agent for in vivo imaging and cancer therapy. **Biomaterials,** v. 51, p. 184-193, 2015. doi: 10.1016/j.biomaterials.2015.01.069.

14 SHAKERI-ZADEH, A. et al. Synergistic effects of magnetic drug targeting using a newly developed nanocapsule and tumor irradiation by ultrasound on CT26 tumors in BALB/c mice. **Journal of Materials Chemistry B,** v. 3, n. 9, p. 1879-1887, 2015.

15 SKIRTACH, A. G. et al. The role of metal nanoparticles in remote release of encapsulated materials. **Nano Letters,** v. 5, n. 7, p. 1371-1377, 2005.

16 TAN, L. et al. Visible light-triggered nitric oxide release from near-infrared fluorescent nanospheric vehicles. **Analyst,** v. 139, n. 13, p. 3398-3406, 2014.

17 LEE, C. S. et al. Endolysosomal environment-responsive photodynamic nanocarrier to enhance cytosolic drug delivery via photosensitizer-mediated membrane disruption. **Biomaterials,** v. 34, n. 36, p. 9227-9236, 2013.

18 XIU, Z.-M. et al. Negligible particle-specific antibacterial activity of silver nanoparticles. **Nano Letters,** v. 12, n. 8, p. 4271-4275, 2012.

19 ZHANG, D. et al. Electromagnetic characteristics and microwave absorption properties of carbon-encapsulated cobalt nanoparticles in 2-18-GHz frequency range. **Carbon,** v. 80, p. 103-111, 2014. doi: 10.1016/j.carbon.2014.08.044

20 MAIA, F. et al. Silica nanocontainers for active corrosion protection. **Nanoscale,** v. 4, n. 4, p. 1287-1298, 2012.

21 SKIRTACH, A. G.; VOLODKIN, D. V.; MOEHWALD, H. Bio-interfaces-interaction of PLL/HA thick films with nanoparticles and microcapsules. **Chemphyschem,** v. 11, n. 4, p. 822-829, 2010.

22 FRENOT, A.; CHRONAKIS, I. S. Polymer nanofibers assembled by electrospinning. **Current Opinion in Colloid & Interface Science,** v. 8, n. 1, p. 64-75, 2003.

23 PHAM, Q. P.; SHARMA, U.; MIKOS, A. G. Electrospinning of polymeric nanofibers for tissue engineering applications: a review. **Tissue Engineering,** v. 12, n. 5, p. 1197-1211, 2006.

24 MA, Z. W. et al. Grafting of gelatin on electrospun poly(caprolactone) nanofibers to improve endothelial cell spreading and proliferation and to control cell orientation. **Tissue Engineering,** v. 11, n. 7-8, p. 1149-1158, 2005.

25 SHEIKH, F. A. et al. Electrospun antimicrobial polyurethane nanofibers containing silver nanoparticles for biotechnological applications. **Macromolecular Research,** v. 17, n. 9, p. 688-696, 2009.

26 HASSIBA, A. J. et al. Review of recent research on biomedical applications of electrospun polymer nanofibers for improved wound healing. **Nanomedicine,** v. 11, n. 6, p. 715-737, 2016.

27 PARK, J. H. et al. Electrospinning fabrication and characterization of poly(vinyl alcohol)/montmorillonite/silver hybrid nanofibers for antibacterial applications. **Colloid and Polymer Science,** v. 288, n. 1, p. 115-121, 2010.

28 MIRANDA, P. B.; DU, Q.; SHEN, Y. R. Interaction of water with a fatty acid Langmuir film. **Chemical Physics Letters,** v. 286, n. 1-2, p. 1-8, 1998.

29 GUZMAN, E. et al. DPPC-DOPC Langmuir monolayers modified by hydrophilic silica nanoparticles: phase behaviour, structure and rheology. **Colloids and Surfaces A:** physicochemical and engineering aspects, v. 413, p. 174-183, 2012. doi: 10.1016/j.colsurfa.2011.12.059

30 NOBRE, T. M. et al. Interactions of bioactive molecules & nanomaterials with Langmuir monolayers as cell membrane models. **Thin Solid Films,** v. 593, p. 158-188, 2015.doi: 10.1016/j.tsf.2015.09.047

31 NOBRE, T. M. et al. Interactions of bioactive molecules & nanomaterials with Langmuir monolayers as cell membrane models. **Thin Solid Films,** v. 593, p. 158-188, 2015. doi: 10.1016/j.tsf.2015.09.047.

32 KRAJEWSKA, B.; WYDRO, P.; JANCZYK, A. Probing the modes of antibacterial activity of chitosan. effects of pH and molecular weight on chitosan interactions with membrane lipids in Langmuir films. **Biomacromolecules,** v. 12, n. 11, p. 4144-4152, 2011.

33 CHENG, C. J. et al. A holistic approach to targeting disease with polymeric nanoparticles. **Nature Reviews Drug Discovery,** v. 14, n. 4, p. 239-247, 2015.

34 CHAN, A. et al. Remote and local control of stimuli responsive materials for therapeutic applications. **Advanced Drug Delivery Reviews,** v. 65, n. 4, p. 497-514, 2013.

35 DUDANI, J. S. et al. Photoactivated spatiotemporally-responsive nanosensors of in vivo protease activity. **Acs Nano,** v. 9, n. 12, p. 11708-11717, 2015.

36 CANFAROTTA, F.; PILETSKY, S. A. Engineered magnetic nanoparticles for biomedical applications. **Advanced Healthcare Materials,** v. 3, n. 2, p. 160-175, 2014.

37 SHUBAYEV, V. I.; PISANIC, T. R.; JIN, S. H. Magnetic nanoparticles for theragnostics. **Advanced Drug Delivery Reviews,** v. 61, n. 6, p. 467-477, 2009.

38 LUK, B. T.; ZHANG, L. F. Cell membrane-camouflaged nanoparticles for drug delivery. **Journal of Controlled Release,** v. 220, p. 600-607, 2015. doi: 10.1016/j.jconrel.2015.07.019

39 KWON, E. J.; LO, J. H.; BHATIA, S. N. Smart nanosystems: bio-inspired technologies that interact with the host environment. **Proceedings of the National Academy of Sciences of the United States of America,** v. 112, n. 47, p. 14460-14466, 2015.

40 WEI, T. et al. A smart antibacterial surface for the on-demand killing and releasing of bacteria. **Advanced Healthcare Materials,** v. 5, n. 4, p. 449-456, 2016.

41 CHIANG, W. L. et al. A rapid drug release system with a NIR light-activated molecular switch for dual-modality photothermal/antibiotic treatments of subcutaneous abscesses. **Journal of Controlled Release,** v. 199, p. 53-62, 2015. doi: 10.1016/j.jconrel.2014.12.011

42 ANDREU, V. et al. Smart dressings based on nanostructured fibers containing natural origin antimicrobial, anti-inflammatory, and regenerative compounds. **Materials,** v. 8, n. 8, p. 5154-5193, 2015.

43 ZHAO, Y. et al. Advanced stimuli-responsive polymer nanocapsules with enhanced capabilities for payloads delivery. **Polymer Chemistry,** v. 6, n. 23, p. 4197-4205, 2015.

44 TORINO, E. et al. Synthesis of semicrystalline nanocapsular structures obtained by thermally induced phase separation in nanoconfinement. **Scientific Reports,** v. 6, p.32727,2016. doi: 10.1038/srep32727

45 LI, Y. L. et al. Biodegradable polymer nanogels for drug/nucleic acid delivery. **Chemical Reviews,** v. 115, n. 16, p. 8564-8608, 2015.

46 CRUCHO, C. I. C. Stimuli-responsive polymeric nanoparticles for nanomedicine. **ChemMedChem,** v. 10, n. 1, p. 24-38, 2015.

47 GARCIA, G. M. et al. Improved nonclinical pharmacokinetics and biodistribution of a new PPAR pan-agonist and COX inhibitor in nanocapsule formulation. **Journal of Controlled Release,** v. 209, p. 207-218, 2015. doi: 10.1016/j.jconrel.2015.04.033

48 BAZYLINSKA, U. et al. Polymeric nanocapsules and nanospheres for encapsulation and long sustained release of hydrophobic cyanine-type photosensitizer. **Colloids and Surfaces A:** physicochemical and engineering aspects**,** v. 442, p. 42-49, 2014. doi: 10.1016/j.colsurfa.2013.02.023

49 XIA, Y. et al. Ag-nanogel blended polymeric membranes with antifouling, hemocompatible and bactericidal capabilities. **Journal of Materials Chemistry B,** v. 3, n. 48, p. 9295-9304, 2015.

50 ESSER-KAHN, A. P. et al. Triggered release from polymer capsules. **Macromolecules,** v. 44, n. 14, p. 5539-5553, 2011.

51 KELLY, K. L. et al. The optical properties of metal nanoparticles: the influence of size, shape, and dielectric environment. **Journal of Physical Chemistry B,** v. 107, n. 3, p. 668-677, 2003.

52 NEAR, R.; HAYDEN, S.; EL-SAYED, M. Extinction vs absorption: which is the indicator of plasmonic field strength for silver nanocubes? **Journal of Physical Chemistry C,** v. 116, n. 43, p. 23019-23026, 2012.

53 YU, L. et al. Enhanced antibacterial activity of silver nanoparticles/halloysite nanotubes/graphene nanocomposites with sandwich-like structure. **Scientific Reports,** v. 4, 2014. doi: 10.1038/srep04551

54 DILL, T. J. et al. Colloidal nanoantennas for hyperspectral chemical mapping. **Acs Nano,** v. 10, n. 8, p. 7523-7531, 2016.

55 MOORES, A.; GOETTMANN, F. The plasmon band in noble metal nanoparticles: an introduction to theory and applications. **New Journal of Chemistry,** v. 30, n. 8, p. 1121-1132, 2006.

56 JAIN, P. K.; EL-SAYED, M. A. Plasmonic coupling in noble metal nanostructures. **Chemical Physics Letters,** v. 487, n. 4-6, p. 153-164, 2010.

57 CREIGHTON, J. A.; EADON, D. G. Ultraviolet visible absorption-spectra of the colloidal metallic elements. **Journal of the Chemical Society:** faraday transactions, v. 87, n. 24, p. 3881-3891, 1991.

58 POTERA, C. Understanding the germicidal effects of silver nanoparticles. **Environmental Health Perspectives,** v. 120, n. 10, p. A386-A386, 2012.

59 FAYAZ, A. M. et al. Biogenic synthesis of silver nanoparticles and their synergistic effect with antibiotics: a study against gram-positive and gram-negative bacteria. **Nanomedicine:**nanotechnology biology and medicine, v. 6, n. 1, p. 103-109, 2010.

60 ABU-YOUSSEF, M. A. M. et al. Synthesis, crystal structure, quantum chemical calculations, DNA interactions, and antimicrobial activity of Ag(2-amino-3-methylpyridine)(2) NO3 and Ag(pyridine-2-carboxaldoxime)NO3. **Inorganic Chemistry,** v. 49, n. 21, p. 9788-9797, 2010.

61 CHATTERJEE, A. et al. Selective fluorogenic and chromogenic probe for detection of silver ions and silver nanoparticles in aqueous media. **Journal of the American Chemical Society,** v. 131, n. 6, p. 2040, 2009.

62 DALLAS, P.; SHARMA, V. K.; ZBORIL, R. Silver polymeric nanocomposites as advanced antimicrobial agents: classification, synthetic paths, applications, and perspectives. **Advances in Colloid and Interface Science,** v. 166, n. 1-2, p. 119-135, 2011.

63 KUMAR, R.; HOWDLE, S.; MUNSTEDT, H. Polyamide/silver antimicrobials: effect of filler types on the silver ion release. **Journal of Biomedical Materials Research Part B:**applied biomaterials, v. 75B, n. 2, p. 311-319, 2005.

64 BATARSEH, K. I. Anomaly and correlation of killing in the therapeutic properties of silver (1) chelation with glutamic and tartaric acids. **Journal of Antimicrobial Chemotherapy,** v. 54, n. 2, p. 546-548, 2004.

65 JUNG, W. K. et al. Antibacterial activity and mechanism of action of the silver ion in Staphylococcus aureus and Escherichia coli. **Applied and Environmental Microbiology,** v. 74, n. 7, p. 2171-2178, 2008.

66 MARTINEZ-CASTANON, G. A. et al. Synthesis and antibacterial activity of silver nanoparticles with different sizes. **Journal of Nanoparticle Research,** v. 10, n. 8, p. 1343-1348, 2008. ISSN 1388-0764.

67 KONG, M. et al. Antimicrobial properties of chitosan and mode of action: a state of the art review. **International Journal of Food Microbiology,** v. 144, n. 1, p. 51-63, 2010.

68 RABEA, E. I. et al. Chitosan as antimicrobial agent: applications and mode of action. **Biomacromolecules,** v. 4, n. 6, p. 1457-1465, 2003.

69 LI, X.-F. et al. Chitosan kills Escherichia coli through damage to be of cell membrane mechanism. **Carbohydrate Polymers,** v. 79, n. 3, p. 493-499, 2010.

70 ARANCIBIA, R. et al. Effects of chitosan particles in periodontal pathogens and gingival fibroblasts. **Journal of Dental Research,** v. 92, n. 8, p. 740-745, 2013.

71 OKAMOTO, Y. et al. Analgesic effects of chitin and chitosan. **Carbohydrate Polymers,** v. 49, n. 3, p. 249-252, 2002.

72 STEJSKAL, J.; TRCHOVA, M. Aniline oligomers versus polyaniline. **Polymer International,** v. 61, n. 2, p. 240-251, 2012.

73 LI, Y. J. et al. Aniline degradation by electrocatalytic oxidation. **Chemosphere,** v. 53, n. 10, p. 1229-1234, 2003.

74 QI, H. et al. Biocompatibility evaluation of aniline oligomers with different end-functional groups. **Toxicology Research,** v. 2, n. 6, p. 427-433, 2013.

75 GUERRY, A. et al. Aniline-catalyzed reductive amination as a powerful method for the preparation of reducing end-"Clickable" chitooligosaccharides. **Bioconjugate Chemistry,** v. 24, n. 4, p. 544-549, 2013.

76 MI, F.-L. et al. Preparation of a silver nanoparticle-based dual-functional sensor using a complexation-reduction method. **Physical Chemistry Chemical Physics,** v. 17, n. 33, p. 21243-21253, 2015.

77 HU, J. et al. Electroactive aniline pentamer cross-linking chitosan for stimulation growth of electrically sensitive cells. **Biomacromolecules,** v. 9, n. 10, p. 2637-2644, 2008.

78 SONG, P. G. et al. Bio-inspired hydrogen-bond cross-link strategy toward strong and tough polymeric materials. **Macromolecules,** v. 48, n. 12, p. 3957-3964, 2015.

79 MATSUMOTO, A. et al. Effect of hydrogen bonds on intermolecular crosslinking reaction by introduction of carboxyl groups in free-radical crosslinking monomethacrylate/dimethacrylate copolymerizations. **European Polymer Journal,** v. 38, n. 9, p. 1777-1782, 2002.

80 SONG, P. A.; XU, Z. G.; GUO, Q. P. Bioinspired strategy to reinforce PVA with improved toughness and thermal properties via hydrogen-bond self-assembly. **Acs Macro Letters,** v. 2, n. 12, p. 1100-1104, 2013.

81 WEI, D. W. et al. The synthesis of chitosan-based silver nanoparticles and their antibacterial activity. **Carbohydrate Research,** v. 344, n. 17, p. 2375-2382, 2009.

82 WEI, Z.; FAUL, C. F. J. Aniline oligomers - architecture, function and new opportunities for nanostructured materials. **Macromolecular Rapid Communications,** v. 29, n. 4, p. 280-292, 2008.

83 WANG, Q. Z. et al. Protonation constants of chitosan with different molecular weight and degree of deacetylation. **Carbohydrate Polymers,** v. 65, n. 2, p. 194-201, 2006.

84 ATKINS, P.; PAULA, J. D.; PETER ATKINS, J. D. P. **Atkins's physical chemistry**. 10th ed. Oxford: Oxford University Press, 2010.

85 YOUNG, R. J.; LOVELL, P. A. **Introduction to polymers**. 3rd ed. Boca Raton: CRC press, 2011.

86 GREULICH, C. et al. Uptake and intracellular distribution of silver nanoparticles in human mesenchymal stem cells. **Acta Biomaterialia,** v. 7, n. 1, p. 347-354, 2011.

87 SOCRATES, G. **Infrared and Raman characteristic group frequencies:** tables and charts. 3rd ed. Chichester: John Wiley & Sons, 2004.

88 THOMAS, S. **Spectroscopic tools.** 2014. Available from:<http://www.science-and-fun.de/tools/>. Accessible at: 02 Apr. 2014.

89 XIA, Y. et al. Surface-engineered nanogel assemblies with integrated blood compatibility, cell proliferation and antibacterial property: towards multifunctional biomedical membranes. **Polymer Chemistry,** v. 5, n. 20, p. 5906-5919, 2014.

90 BOSWORTH, L. A.; DOWNES, S. Physicochemical characterisation of degrading polycaprolactone scaffolds. **Polymer Degradation and Stability,** v. 95, n. 12, p. 2269-2276, 2010.

91 LABET, M.; THIELEMANS, W. Synthesis of polycaprolactone: a review. **Chemical Society Reviews,** v. 38, n. 12, p. 3484-3504, 2009.

92 SAHOO, S. et al. Growth factor delivery through electrospun nanofibers in scaffolds for tissue engineering applications. **Journal of Biomedical Materials Research Part A,** v. 93A, n. 4, p. 1539-1550, 2010.

93 WUTTICHAROENMONGKOL, P. et al. Preparation and characterization of novel bone scaffolds based on electrospun polycaprolactone fibers filled with nanoparticles. **Macromolecular Bioscience,** v. 6, n. 1, p. 70-77, 2006.

94 LEE, H.; YOON, H.; KIM, G. Highly oriented electrospun polycaprolactone micro/nanofibers prepared by a field-controllable electrode and rotating collector. **Applied Physics A:**materials science & processing, v. 97, n. 3, p. 559-565, 2009.

95 HOHMAN, M. M. et al. Electrospinning and electrically forced jets. I. stability theory. **Physics of Fluids,** v. 13, n. 8, p. 2201-2220, 2001.

96 SHIN, Y. M. et al. Experimental characterization of electrospinning: the electrically forced jet and instabilities. **Polymer,** v. 42, n. 25, p. 9955-9967, 2001.

97 SHIN, Y.M. et al. Electrospinning: a whipping fluid jet generates submicron polymer fibers. **Applied Physics Letters,** v. 78, n. 8, p. 1149-1151, 2001.

98 MERCANTE, L. A. et al. Electrospinning-based (bio)sensors for food and agricultural applications: a review. **Trends in Analytical Chemistry,** v.91, p,91-103, 2017. doi.org/10.1016/j.trac.2017.04.004

99 PASTORIZA-SANTOS, I.; LIZ-MARZAN, L. M. Synthesis of silver nanoprisms in DMF. **Nano Letters,** v. 2, n. 8, p. 903-905, 2002.

100 KU, S. H.; PARK, C. B. Human endothelial cell growth on mussel-inspired nanofiber scaffold for vascular tissue engineering. **Biomaterials,** v. 31, n. 36, p. 9431-9437, 2010.

101 YOO, H. S.; KIM, T. G.; PARK, T. G. Surface-functionalized electrospun nanofibers for tissue engineering and drug delivery. **Advanced Drug Delivery Reviews,** v. 61, n. 12, p. 1033-1042, 2009.

102 JUNG, D. et al. Incorporation of functionalized gold nanoparticles into nanofibers for enhanced attachment and differentiation of mammalian cells. **Journal of Nanobiotechnology,** v. 10, n.23, p. 1-10,2012. doi: 10.1186/1477-3155-10-23.

103 GLINEL, K. et al. Antibacterial and antifouling polymer brushes incorporating antimicrobial peptide. **Bioconjugate Chemistry,** v. 20, n. 1, p. 71-77, 2009.

104 PANTHI, G. et al. Electrospun composite nanofibers of polyacrylonitrile and Ag2CO3 nanoparticles for visible light photocatalysis and antibacterial applications. **Journal of Materials Science,** v. 50, n. 13, p. 4477-4485, 2015.

105 KUMAR, A. et al. Antibacterial efficacy of 405, 460 and 520 nm light emitting diodes on Lactobacillus plantarum, Staphylococcus aureus and Vibrio parahaemolyticus. **Journal of Applied Microbiology,** v. 120, n. 1, p. 49-56, 2016.

106 PERNI, S. et al. Nanoparticles: their potential use in antibacterial photodynamic therapy. **Photochemical & Photobiological Sciences,** v. 10, n. 5, p. 712-720, 2011.

107 RHODES, N. L. R. et al. Violet 405nm light: a novel therapeutic agent against -lactam-resistant Escherichia coli. **Lasers in Surgery and Medicine,** v. 48, n. 3, p. 311-317, 2016.

108 GHATE, V. et al. Enhancing the antibacterial effect of 461 and 521 nm light emitting diodes on selected foodborne pathogens in trypticase soy broth by acidic and alkaline pH conditions. **Food Microbiology,** v. 48, p. 49-57, 2015. doi: 10.1016/j.fm.2014.10.014

109 GHATE, V. S. et al. Antibacterial effect of light emitting diodes of visible wavelengths on selected foodborne pathogens at different illumination temperatures. **International Journal of Food Microbiology,** v. 166, n. 3, p. 399-406, 2013.

110 MACLEAN, M. et al. 405 nm light technology for the inactivation of pathogens and its potential role for environmental disinfection and infection control. **Journal of Hospital Infection,** v. 88, n. 1, p. 1-11, 2014.

111 FAZIO, E. et al. Laser light triggered smart release of silibinin from a PEGylated-PLGA gold nanocomposite. **Journal of Materials Chemistry B,** v. 3, n. 46, p. 9023-9032, 2015.

112 BLACK, K. C. L. et al. Bacterial killing by light-triggered release of silver from biomimetic metal nanorods. **Small,** v. 10, n. 1, p. 169-178, 2014.

113 JORGENSEN, J. H.; FERRARO, M. J. Antimicrobial susceptibility testing: a review of general principles and contemporary practices. **Clinical Infectious Diseases,** v. 49, n. 11, p. 1749-1755, 2009.

114 MULVANEY, P. Surface plasmon spectroscopy of nanosized metal particles. **Langmuir,** v. 12, n. 3, p. 788-800, 1996.

115 NIIKURA, K. et al. Sub-100 nm Gold nanoparticle vesicles as a drug delivery carrier enabling rapid drug release upon light irradiation. **Acs Applied Materials & Interfaces,** v. 5, n. 9, p. 3900-3907, 2013.

116 COBLEY, C. M. et al. Shape-controlled synthesis of silver nanoparticles for plasmonic and sensing applications. **Plasmonics,** v. 4, n. 2, p. 171-179, 2009.

117 ESHRAGHI, S.; DAS, S. Mechanical and microstructural properties of polycaprolactone scaffolds with one-dimensional, two-dimensional, and three-dimensional orthogonally oriented porous architectures produced by selective laser sintering. **Acta Biomaterialia,** v. 6, n. 7, p. 2467-2476, 2010.

118 DASH, T. K.; KONKIMALLA, V. B. Poly-epsilon-caprolactone based formulations for drug delivery and tissue engineering: a review. **Journal of Controlled Release,** v. 158, n. 1, p. 15-33, 2012.

119 SONDI, I.; SALOPEK-SONDI, B. Silver nanoparticles as antimicrobial agent: a case study on E-coli as a model for Gram-negative bacteria. **Journal of Colloid and Interface Science,** v. 275, n. 1, p. 177-182, 2004.

120 FENG, Q. L. et al. A mechanistic study of the antibacterial effect of silver ions on Escherichia coli and Staphylococcus aureus. **Journal of Biomedical Materials Research,** v. 52, n. 4, p. 662-668, 2000.

121 CELEBIOGLU, A. et al. One-step synthesis of size-tunable Ag nanoparticles incorporated in electrospun PVA/cyclodextrin nanofibers. **Carbohydrate Polymers,** v. 99, p. 808-816, 2014. doi: 10.1016/j.carbpol.2013.08.097.

122 LEE, S. J. et al. Electrospun chitosan nanofibers with controlled levels of silver nanoparticles. preparation, characterization and antibacterial activity. **Carbohydrate Polymers,** v. 111, p. 530-537, 2014. doi: 10.1016/j.carbpol.2014.04.026.

123 LIU, C. et al. Development and antibacterial performance of novel polylactic acid-graphene oxide-silver nanoparticle hybrid nanocomposite mats prepared by electrospinning. **Acs Biomaterials Science & Engineering,** v. 3, n. 3, p. 471-486, 2017.

124 SAQUING, C. D.; MANASCO, J. L.; KHAN, S. A. Electrospun nanoparticle-nanofiber composites via a one-step synthesis. **Small,** v. 5, n. 8, p. 944-951, 2009.

125 KALWAR, K. et al. Coaxial electrospinning of polycaprolactone@chitosan: characterization and silver nanoparticles incorporation for antibacterial activity. **Reactive & Functional Polymers,** v. 107, p. 87-92, 2016. doi: 10.1016/j.reactfunctpolym.2016.08.010

126 ANNUR, D. et al. Plasma-synthesized silver nanoparticles on electrospun chitosan nanofiber surfaces for antibacterial applications. **Biomacromolecules,** v. 16, n. 10, p. 3248-3255, 2015.

127 CHEN, D. W. C.; LIU, S. J. Nanofibers used for delivery of antimicrobial agents. **Nanomedicine,** v. 10, n. 12, p. 1959-1971, 2015.

128 WU, J. et al. Silver nanoparticle/bacterial cellulose gel membranes for antibacterial wound dressing: investigation in vitro and in vivo. **Biomedical Materials,** v. 9, n. 3, 2014.

129 AZIZ, Z.; ABU, S. F.; CHONG, N. J. A systematic review of silver-containing dressings and topical silver agents (used with dressings) for burn wounds. **Burns,** v. 38, n. 3, p. 307-318, 2012.

130 ABRIGO, M.; MCARTHUR, S. L.; KINGSHOTT, P. Electrospun nanofibers as dressings for chronic wound care: advances, challenges, and future prospects. **Macromolecular Bioscience,** v. 14, n. 6, p. 772-792, 2014.

131 BROCKMAN, H. Lipid monolayers: why use half a membrane to characterize protein-membrane interactions? **Current Opinion in Structural Biology,** v. 9, n. 4, p. 438-443, 1999.

132 TREDGOLD, R. H. An introduction to ultrathin organic films - from Langmuir-Blodgett to self-assembly. **Nature,** v. 354, n. 6349, p. 120-120, 1991.

133 PETERSON, I. R. Langmuir-Blodgett films. **Journal of Physics D:** applied physics, v. 23, n. 4, p. 379-395, 1990.

134 GINER-CASARES, J. J.; BREZESINSKI, G.; MOHWALD, H. Langmuir monolayers as unique physical models. **Current Opinion in Colloid &amp:** interface science, v. 19, n. 3, p. 176-182, 2014.

135 TORRANO, A. A. et al. Probing the interaction of oppositely charged gold nanoparticles with DPPG and DPPC Langmuir monolayers as cell membrane models. **Colloids and Surfaces B:** biointerfaces, v. 108, p. 120-126, 2013. doi: 10.1016/j.colsurfb.2013.02.014.

136 STEFANIU, C.; BREZESINSKI, G.; MOHWALD, H. Langmuir monolayers as models to study processes at membrane surfaces. **Advances in Colloid and Interface Science,** v. 208, p. 197-213, 2014. doi: 10.1016/j.cis.2014.02.013.

137 LIU, X. T.; CHEN, K. L. Interactions of graphene oxide with model cell membranes: probing nanoparticle attachment and lipid bilayer disruption. **Langmuir,** v. 31, n. 44, p. 12076-12086, 2015.

138 FERREIRA, J. V. N. et al. Mechanism of action of thymol on cell membranes investigated through lipid langmuir monolayers at the air-water interface and molecular simulation. **Langmuir,** v. 32, n. 13, p. 3234-3241, 2016.

139 MOHWALD, H. Direct characterization of monolayers at the air water interface. **Thin Solid Films,** v. 159, p. 1-15, 1988. doi: 10.1016/0040-6090(88)90612-8.

140 VOLLHARDT, D.; FAINERMAN, V. B.; SIEGEL, S. Thermodynamic and textural characterization of DPPG phospholipid monolayers. **Journal of Physical Chemistry B,** v. 104, n. 17, p. 4115-4121, 2000.

141 AVANTI LIPIDS POLAR. 2017. Available from: < https://avantilipids.com/ >. Accessible at: 15 Apr. 2014.

142 HARRISON, J. J. et al. Microtiter susceptibility testing of microbes growing on peg lids: a miniaturized biofilm model for high-throughput screening. **Nature Protocols,** v. 5, n. 7, p. 1236-1254, 2010.

143 LI, W. R. et al. Antibacterial activity and mechanism of silver nanoparticles on Escherichia coli. **Applied Microbiology and Biotechnology,** v. 85, n. 4, p. 1115-1122, 2010.

144 AKBARZADEH, A. et al. Liposome: classification, preparation, and applications. **Nanoscale Research Letters,** v. 8, n.1, p.102,2013. doi: 10.1186/1556-276X-8-102.

145 PAVINATTO, F. J. et al. Probing chitosan and phospholipid interactions using Langmuir and Langmuir-Blodgett films as cell membrane models. **Langmuir,** v. 23, n. 14, p. 7666-7671, 2007.

146 GARIDEL, P.; BLUME, A. Miscibility of phosphatidylethanolamine-phosphatidylglycerol mixtures as a function of pH and acyl chain length. **European Biophysics Journal:** with Biophysics Letters, v. 28, n. 8, p. 629-638, 2000.

Appendix

The electronic circuits of the LASER and LED systems consist of a voltage source that supplies 12 V to the current source. It is configured with a current for the LASER and LED of 83 mA and 70 mA, respectively, yielding a power density of irradiation of approximately 32 $mWcm^{-2}$.

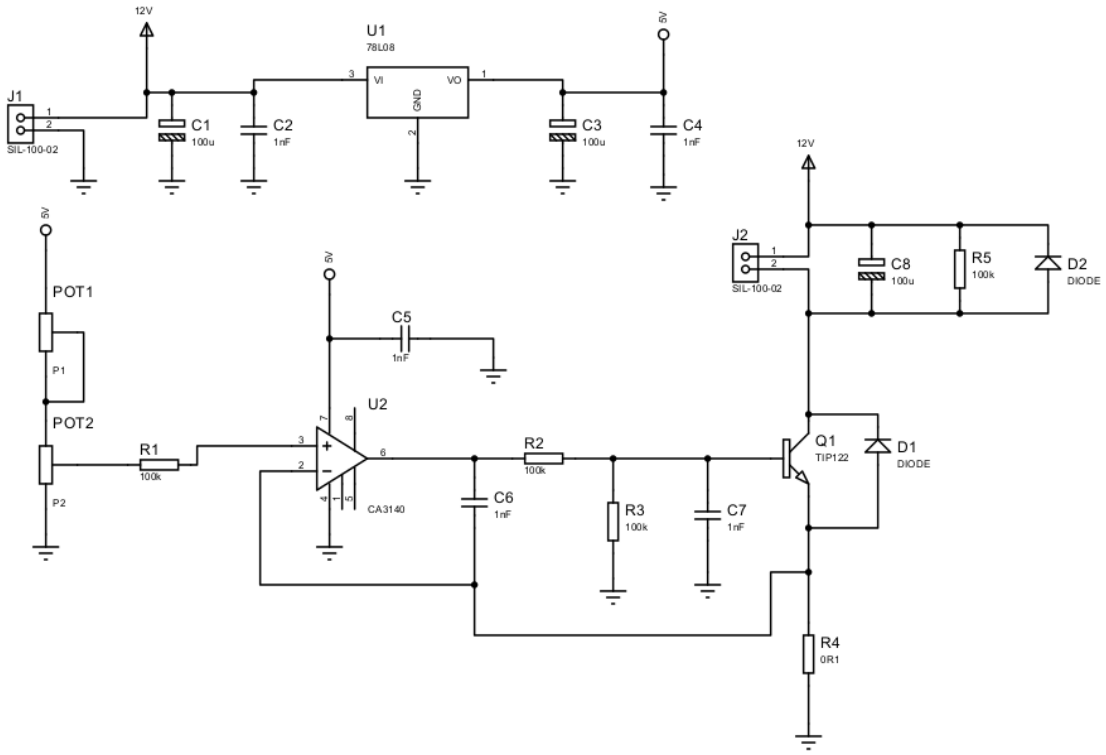

Figure 7.1 - Electronic circuits of the LASER and LED systems.

Source: By the author.